Oxetane-based Polyketide Surrogate to Probe Regio-specificity of a Polyketide Synthase

Bryan D. Ellis[1†], Jacob C. Milligan[2†], Alexander R. White[1], Vy Duong[3], Pilar X. Altman[2], Lina Y. Mohammed[4], Matthew P. Crump[4], John Crosby[4], Ray Luo[3], Christopher D. Vanderwal,[1*] Shiou-Chuan Tsai[2*]

[1]1102 Natural Sciences II, Department of Chemistry, University of California, Irvine, 92697-2025, USA

[2]2218 Natural Sciences I, Departments of Molecular Biology and Biochemistry, Chemistry, and Pharmaceutical Sciences, University of California, Irvine, CA 92697

[3]3206 Natural Sciences I, Departments of Molecular Biology and Biochemistry, Biomedical Engineering, and Chemical Engineering & Materials Science, University of California, Irvine, CA 92697

[4]School of Chemistry, University of Bristol, Cantock's Close, Bristol, BS8 1TS, United Kingdom.

Supporting Information Placeholder

ABSTRACT: Polyketides are a large class of bioactive natural products with a wide range of structures and functions. Polyketides are biosynthesized by large, multi-domain enzyme complexes termed polyketide synthases (PKSs). One of the primary challenges when studying PKSs is the high reactivity of their poly-β-ketone substrates. This has hampered structural and mechanistic characterization of PKS-polyketide complexes, and, as a result, little is known about how PKSs position the unstable substrates for proper catalysis while displaying high levels of regio- and stereospecificity. Here we describe the development and application of an oxetane-based PKS substrate mimic. This enabled the first structural determination of the acyl-enzyme intermediate of a ketosynthase (KS) in complex with an inert extender unit mimic. The crystal structure, in combination with molecular dynamics simulations, led to a proposed mechanism for the unique activity of DpsC, the priming ketosynthase for daunorubicin biosynthesis. The successful application of an oxetane-based polyketide mimic suggests that this novel class of probes could have wide-ranging applications to the greater biosynthetic community.

Polyketide natural products are a large and diverse class of secondary metabolites of high impact to human health.[1-2] Type II polyketides are biosynthesized by a type II polyketide synthase (PKS) consisting of 5–10 stand-alone enzymes that form complexes in solution.[3] Notable examples include actinorhodin, daunorubicin, and tetracenomycin C (**Figure 1A**).[4-6] PKSs have been heavily studied because of their ability to efficiently biosynthesize complex small molecules and their potential to be engineered for combinatorial biosynthesis.[1-2]

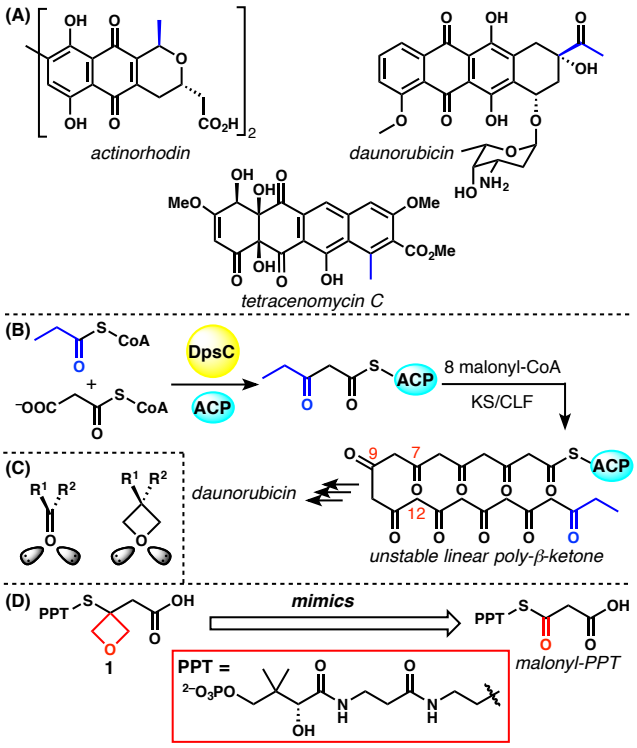

Figure 1. (A) Examples of type II polyketides with the starter units shown in blue. (B) DpsC catalyzes the transfer of small acyl-CoAs, including propionyl-CoA, to the acyl carrier protein (ACP) and also the initial chain elongation reaction that condenses the propionyl starter unit with malonyl-ACP to afford the growing intermediate. Eight more rounds of chain elongation produce the unstable, linear poly-β-ketone intermediate that is cyclized and tailored to become daunorubicin. (C) Oxetanes are isosteres for the carbonyl group. (D) Probe **1**, with the thioester carbonyl group replaced by an oxetane, mimics malonyl-PPT.

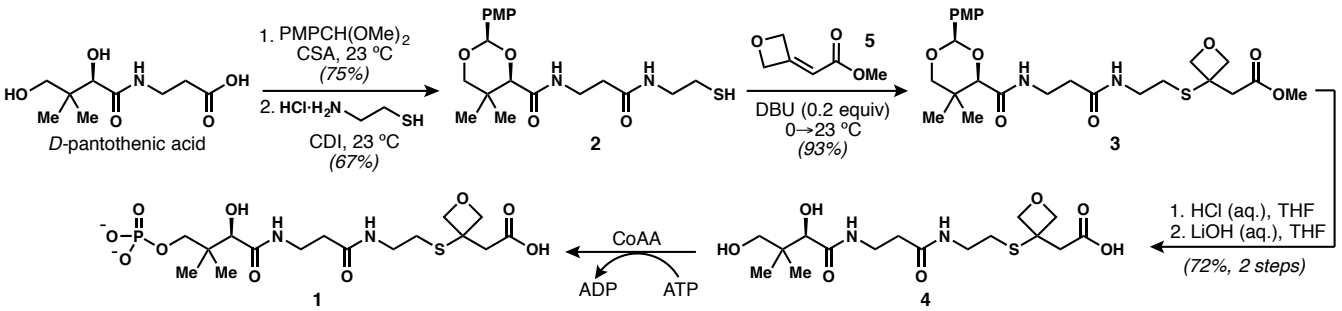

Scheme 1. Synthesis of malonyl-PPT probe **1**

One of the primary challenges associated with investigating type II PKS is the high reactivity of enzymatic substrates and intermediates.[7] The poly-β-ketone generated by most type II PKSs is highly susceptible to spontaneous, non-specific cyclization, which has made structural studies of PKS-substrate complexes extremely difficult (**Figure 1B**).[8] Without this structural knowledge, rational engineering of substrate specificity often leads to inactive enzymes.[3] Our group previously synthesized isoxazole-based polyketide isosteres and applied them to the characterization of the interior pocket of an acyl carrier protein.[9] Given the substantial structural differences between these first-generation chemical probes and the natural poly-β-ketone substrates, we expect their applications to be rather limited. To interrogate PKS-substrate complexes more broadly, we sought to generate probe molecules that more closely mimicked the natural substrates.

The oxetane ring is well recognized as an isostere for the carbonyl group,[10] owing primarily to the efforts of Carreira, Müller, and co-workers.[11-18] Although slightly larger than the carbonyl, the oxetane orients its oxygen lone pairs along similar vectors to a carbonyl group (**Figure 1C**). To date, this carbonyl–oxetane replacement strategy has not been used to study questions in polyketide biosynthesis where it is ideally suited for strategic replacement of carbonyl groups in unstable poly-β-ketone intermediates of aromatic polyketides.

Here we present the synthesis of an oxetane-based PKS substrate mimic **1** (**Figure 1D**) and demonstrate its applicability by co-crystallizing it with the enzyme DpsC from the daunorubicin type II PKS from *Streptomyces peucetius*.[19-22] DpsC is a unique enzyme that has both acyltransferase (AT) and priming ketosynthase (ketosynthase III, KS III) activities.[20-22] However, the structural basis for the unique dual activity of DpsC is unclear because of the lack of high-resolution substrate-DpsC structures. Here we present a co-crystal structure and molecular dynamics (MD) simulations that provide mechanistic insight into the KS activity of this enzyme.

Phosphopantetheine (PPT) malonate mimic **1** was synthesized from commercially available *D*-pantothenic acid (**Scheme 1**). Acetal formation, followed by a CDI-mediated amide coupling with cysteamine hydrochloride produced thiol **2**. The 1,3-diketone surrogate was installed via base-catalyzed thia-Michael addition of **2** to oxetane-bearing enoate **5**, yielding **3**.[13] Acetal hydrolysis and ester saponification of **3** unveiled the diol and carboxylic acid moieties, respectively, and provided the penultimate intermediate **4**. The synthesis of **1** was completed using chemoenzymatic phosphorylation.[23]

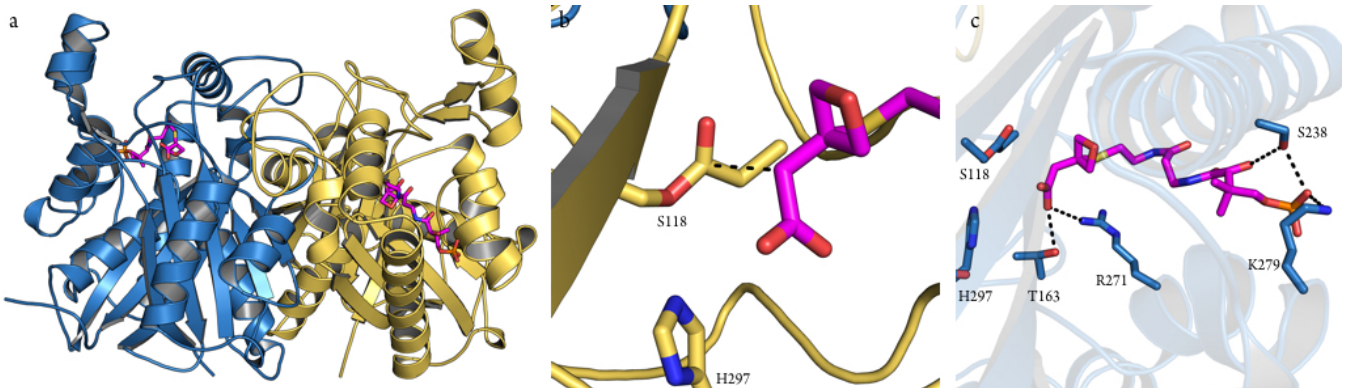

Figure 2. Crystal structure of propionyl-DpsC bound to extender unit mimic **1**. (a) Overall structure of the dimeric propionyl-DpsC in complex with **1**. The DpsC monomers are shown in blue and gold, and **1** is shown in magenta. (b) S118 is shown with its propionylated side chain with the carbon bond that would be formed shown as a black dashed line. (c) Overview of DpsC-**1** interactions within the active site and near the enzyme surface.

The DpsC-**1** model therefore provides new insights into the positioning of substrates just prior to catalysis. As expected, the Asp-His-Ser catalytic triad forms a hydrogen bond network that results in an activated S118 nucleophile (see Figure S4 for details). The resulting propionyl-serine side chain is in close proximity to probe **1**. In particular, the two carbon atoms that would normally participate in the Claisen condensation reaction were separated by an appropriate distance (2.9 Å) and were aligned appropriately (**Figure 2**). The carboxylate of **1** interacts with R271 via a charge-charge interaction and has a hydrogen bond with T163 (**Figure 2C**). The terminal phosphate shows a charge-charge interaction with K279 as well as a hydrogen bond to S238, which is consistent with many other PKS enzymes that use positively charged surface residues to position the phosphate moiety of the phosphopantetheine prosthetic group.[3, 8]

Canonical KSIIIs use conserved residues in an oxyanion hole to stabilize the buildup of negative charge on the thioester carbonyl.[3, 8] Residues H244 and N274 in the prototypical KSIII FabH, known to be essential for decarboxylation,[24-25] are not conserved in DpsC. In the DpsC-**1** structure, the oxetane oxygen atom did not orient itself into a positively charged environment within the DpsC active site (**Figure 2C**). The structurally equivalent positions in DpsC are P265, which does not contain a suitable side chain for oxy-anion stabilization, and H297 is locked in a hydrogen bond network with D302 and S118. The side chain of H198 is within the active site and could potentially stabilize an oxyanion; however, the oxygen of the oxetane group is pointing away from this side chain in the crystal structure. One possibility is that substrate decarboxylation and formation of the enolate intermediate reorients the oxygen towards H198 via a simple bond rotation to stabilize the newly-formed negative charge (**Figure S4**). This proposed mechanism is currently under investigation.

To further assess the validity of the carbonyl-oxetane replacement strategy, the atomic coordinates of the co-crystal structure were used to parameterize and generate two types of MD simulations for comparison: DpsC bound to either oxetane-based probe **1** or the more natural, malonate-PPT (**Figure 1C**). The same atomic coordinates of the co-crystal structure were used to generate the MD simulation for DpsC bound to malonyl-PPT, in which the oxetane substituent was mutated *in silico* into a carbonyl group. Trajectories of both systems in explicit solvent were collected over a microsecond for comparative analyses of relative binding affinity, backbone fluctuations and low-frequency motions. These simulations demonstrated similar relative binding affinities, overall long-term motion and high-frequency movement of binding site residues (**Figures S5–S10**). This provides further support that the protein conformation, substrate-DpsC interactions, as well as protein dynamics near the interacting residues between DpsC and probe **1** are self-consistent.

In summary, we report the first design, synthesis and application of an oxetane-based probe as a surrogate for the carbonyl group of an electrophilic thioester. This study clarifies how the substrate is oriented for DpsC-catalyzed decarboxylation of malonyl-CoA. More generally, this study provides a proof-of-concept of our use of oxetane isosteres to investigate polyketide synthesis. Ongoing efforts include the synthesis of higher-order poly-β-ketone mimics that contain multiple carbonyl to oxetane substitutions, which are currently being applied in mechanistic and structural analyses of other iterative PKSs. These polyketide mimics will enable investigations of important substrate-enzyme and protein-protein interactions that govern the efficiency and selectivity of PKSs, ultimately leading to advances in molecular design and medicinal chemistry.

Supporting Information. A pdf file of Supporting Information is available free of charge on the ACS Publications website

Corresponding Author
cdv@uci.edu, sctsai@uci.edu
Author Contributions
[†]These authors contributed equally to this work.

ACKNOWLEDGMENT

This work was funded by NIH GM100305 and GM076330 (to S.-C.T.) and by NSF CHE-1564340 (to C.D.V.). This work was part of the DOE Joint BioEnergy Institute supported by the U. S. Department of Energy, Office of Science, Office of Biological and Environmental Research, through contract DE-AC02-05CH11231 between Lawrence Berkeley National Laboratory and the U. S. Department of Energy. Use of the Stanford Synchrotron Radiation Lightsource, SLAC National Accelerator Laboratory, is supported by the U.S. Department of Energy, Office of Science, Office of Basic Energy Sciences under Contract No. DE-AC02-76SF00515. The SSRL Structural Molecular Biology Program is supported by the DOE Office of Biological and Environmental Research, and by the National Institutes of Health, National Institute of General Medical Sciences (including P41GM103393). Kostas Vasilakis and Pakorn Wattana-Amorn are acknowledged for their assistance with cloning of the dps PKS.

REFERENCES

1. Staunton, J.; Weissman, K. J., Polyketide biosynthesis: a millennium review. *Nat Prod Rep* **2001,** *18* (4), 380-416.
2. Borchardt, J. K., Combinatorial Biosynthesis: Panning for Pharmaceutical Gold. *Modern Drug Discovery* **1999,** *2* (4), 22-29.
3. Das, A.; Khosla, C., Biosynthesis of aromatic polyketides in bacteria. *Acc Chem Res* **2009,** *42* (5), 631-639.
4. Kim, E. S.; Bibb, M. J.; Butler, M. J.; Hopwood, D. A.; Sherman, D. H., Sequences of the oxytetracycline

polyketide synthase-encoding otc genes from Streptomyces rimosus. *Gene* **1994,** *141* (1), 141-142.
5. Motamedi, H.; Hutchinson, C. R., Cloning and heterologous expression of a gene cluster for the biosynthesis of tetracenomycin C, the anthracycline antitumor antibiotic of Streptomyces glaucescens. *Proc Natl Acad Sci U S A* **1987,** *84* (13), 4445-4449.
6. Malpartida, F.; Hopwood, D. A., Molecular cloning of the whole biosynthetic pathway of a Streptomyces antibiotic and its expression in a heterologous host. *Nature* **1984,** *309* (5967), 462-464.
7. Harris, T. M.; Harris, C. M.; Hindley, K. B., Biogenetic-type syntheses of polyketide metabolites. *Fortschr Chem Org Naturst* **1974,** *31* (0), 217-282.
8. Tsai, S. C.; Ames, B. D., Structural enzymology of polyketide synthases. *Methods Enzymol* **2009,** *459*, 17-47.
9. Shakya, G.; Rivera, H., Jr.; Lee, D. J.; Jaremko, M. J.; La Clair, J. J.; Fox, D. T.; Haushalter, R. W.; Schaub, A. J.; Bruegger, J.; Barajas, J. F.; White, A. R.; Kaur, P.; Gwozdziowski, E. R.; Wong, F.; Tsai, S. C.; Burkart, M. D., Modeling linear and cyclic PKS intermediates through atom replacement. *J Am Chem Soc* **2014,** *136* (48), 16792-16799.
10. Bull, J. A.; Croft, R. A.; Davis, O. A.; Doran, R.; Morgan, K. F., Oxetanes: Recent Advances in Synthesis, Reactivity, and Medicinal Chemistry. *Chem Rev* **2016,** *116* (19), 12150-12233.
11. Burkhard, J. A.; Tchitchanov, B. H.; Carreira, E. M., Cascade formation of isoxazoles: facile base-mediated rearrangement of substituted oxetanes. *Angew Chem Int Ed Engl* **2011,** *50* (23), 5379-5382.
12. Burkhard, J. A.; Wuitschik, G.; Plancher, J. M.; Rogers-Evans, M.; Carreira, E. M., Synthesis and stability of oxetane analogs of thalidomide and lenalidomide. *Org Lett* **2013,** *15* (17), 4312-4315.
13. Burkhard, J. A.; Wuitschik, G.; Rogers-Evans, M.; Muller, K.; Carreira, E. M., Oxetanes as versatile elements in drug discovery and synthesis. *Angew Chem Int Ed Engl* **2010,** *49* (48), 9052-9067.
14. McLaughlin, M.; Yazaki, R.; Fessard, T. C.; Carreira, E. M., Oxetanyl peptides: novel peptidomimetic modules for medicinal chemistry. *Org Lett* **2014,** *16* (16), 4070-4073.
15. Rogers-Evans, M.; Knust, H.; Plancher, J. M.; Carreira, E. M.; Wuitschik, G.; Burkhard, J.; Li, D. B.; Guerot, C., Adventures in drug-like chemistry space: from oxetanes to spiroazetidines and beyond! *Chimia (Aarau)* **2014,** *68* (7-8), 492-499.
16. Ruider, S. A.; Muller, S.; Carreira, E. M., Ring expansion of 3-oxetanone-derived spirocycles: facile synthesis of saturated nitrogen heterocycles. *Angew Chem Int Ed Engl* **2013,** *52* (45), 11908-11911.
17. Wuitschik, G.; Rogers-Evans, M.; Buckl, A.; Bernasconi, M.; Marki, M.; Godel, T.; Fischer, H.; Wagner, B.; Parrilla, I.; Schuler, F.; Schneider, J.; Alker, A.; Schweizer, W. B.; Muller, K.; Carreira, E. M., Spirocyclic oxetanes: synthesis and properties. *Angew Chem Int Ed Engl* **2008,** *47* (24), 4512-4515.
18. Wuitschik, G.; Rogers-Evans, M.; Muller, K.; Fischer, H.; Wagner, B.; Schuler, F.; Polonchuk, L.; Carreira, E. M., Oxetanes as promising modules in drug discovery. *Angew Chem Int Ed Engl* **2006,** *45* (46), 7736-7739.
19. Grimm, A.; Madduri, K.; Ali, A.; Hutchinson, C. R., Characterization of the Streptomyces peucetius ATCC 29050 genes encoding doxorubicin polyketide synthase. *Gene* **1994,** *151* (1-2), 1-10.
20. Bao, W.; Sheldon, P. J.; Hutchinson, C. R., Purification and properties of the Streptomyces peucetius DpsC beta-ketoacyl:acyl carrier protein synthase III that specifies the propionate-starter unit for type II polyketide biosynthesis. *Biochemistry* **1999,** *38* (30), 9752-9757.
21. Bao, W.; Sheldon, P. J.; Wendt-Pienkowski, E.; Hutchinson, C. R., The Streptomyces peucetius dpsC gene determines the choice of starter unit in biosynthesis of the daunorubicin polyketide. *J Bacteriol* **1999,** *181* (15), 4690-4695.
22. Rajgarhia, V. B.; Priestley, N. D.; Strohl, W. R., The product of dpsC confers starter unit fidelity upon the daunorubicin polyketide synthase of Streptomyces sp. strain C5. *Metab Eng* **2001,** *3* (1), 49-63.
23. Yang, K.; Eyobo, Y.; Brand, L. A.; Martynowski, D.; Tomchick, D.; Strauss, E.; Zhang, H., Crystal structure of a type III pantothenate kinase: insight into the mechanism of an essential coenzyme A biosynthetic enzyme universally distributed in bacteria. *J Bacteriol* **2006,** *188* (15), 5532-5540.
24. Davies, C.; Heath, R. J.; White, S. W.; Rock, C. O., The 1.8 A crystal structure and active-site architecture of beta-ketoacyl-acyl carrier protein synthase III (FabH) from escherichia coli. *Structure* **2000,** *8* (2), 185-195.
25. Sachdeva, S.; Musayev, F.; Alhamadsheh, M. M.; Neel Scarsdale, J.; Tonie Wright, H.; Reynolds, K. A., Probing reactivity and substrate specificity of both subunits of the dimeric Mycobacterium tuberculosis FabH using alkyl-CoA disulfide inhibitors and acyl-CoA substrates. *Bioorg Chem* **2008,** *36* (2), 85-90.

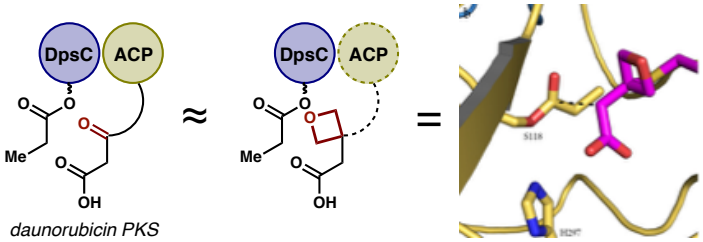

daunorubicin PKS

An Oxetane-based Polyketide Surrogate to Probe Substrate Binding in a Polyketide Synthase

Bryan D. Ellis[1†], Jacob C. Milligan[2†], Alexander R. White[2], Vy Duong[3], Pilar X. Altman[2], Lina Y. Mohammed[4], Matthew P. Crump[4], John Crosby[4], Ray Luo[3], Christopher D. Vanderwal,[1*] Shiou-Chuan Tsai[2*]

[1]1102 Natural Sciences II, Department of Chemistry, University of California, Irvine, 92697-2025, USA
[2]2218 Natural Sciences I, Departments of Molecular Biology and Biochemistry, Chemistry, and Pharmaceutical Sciences, University of California, Irvine, CA 92697
[3]3206 Natural Sciences I, Departments of Molecular Biology and Biochemistry, Biomedical Engineering, and Chemical Engineering & Materials Science, University of California, Irvine, CA 92697
[4]School of Chemistry, University of Bristol, United Kingdom, Bristol BS8 1TS, United Kingdom.

Supporting Information

Table of Contents:

I. Materials and Methods.

All reactions were carried out in flame- or oven-dried glassware under a positive pressure of argon (Ar), unless otherwise noted. Dry acetonitrile (MeCN), dichloromethane (CH_2Cl_2), diethyl ether (Et_2O), tetrahydrofuran (THF), and dimethylformamide (DMF) were obtained by passage of the solvents through a column of neutral alumina under an atmosphere of argon. No precautions were made towards extruding air in aqueous media, unless otherwise noted. Solvents used for workup and chromatography such as CH_2Cl_2, ethyl acetate (EtOAc), hexanes, pentanes, and methanol were used as received from their respective suppliers. Reagents were used as received by their respective suppliers unless otherwise noted. Reactions were monitored by analytical thin-layer chromatography (TLC) using Merck 60 F_{254} glass-backed silica gel (SiO_2) TLC plates. TLC plates were visualized with UV irradiation (254 nm) and treatment with *p*-anisaldehyde or $KMnO_4/H_2SO_4$. Flash chromatography was performed on EMD 60 Å (40–63 μm) mesh SiO_2. NMR spectra were collected on Bruker GN500, CRYO500, or AVANCE600 instruments. ^{1}H and ^{13}C NMR spectra are referenced using the signal(s) of the residual undeuterated solvent. All spectra were collected at 298 K, unless otherwise indicated. Chemical shifts are reported in parts per million (ppm) and multiplicities are abbreviated as follows: s (singlet), d (doublet), t (triplet), q (quartet), quin (quintet), sept (septet), m (multiplet), br (broad), ap (apparent). Coupling constants (*J*) are reported in Hertz (Hz). Infrared (IR) spectra were collected on a Varian 640-IR spectrometer and peaks are recorded in cm^{-1}. High resolution mass spectra (HRMS) were obtained using a Walters LCT Premier spectrometer using electrospray ionization-time of flight (ESI) or chemical ionization-time of flight (CI).

II. List of Abbreviations

AcOH	acetic acid
ADP	adenosine diphosphate
ATP	adenosine triphosphate
CDI	1,1'-carbonyldiimidazole
CSA	10-camphorsulfonic acid
DBU	1,8-diazabicyclo[5.4.0]undec-7-ene

Et_2O	diethyl ether
EtOAc	ethyl acetate
LRMS	low resolution mass spectrometry
MeCN	acetonitrile
MeOH	methanol
PMP	*p*-methoxyphenyl
THF	tetrahydrofuran

III. Experimental Procedures and Characterization Data

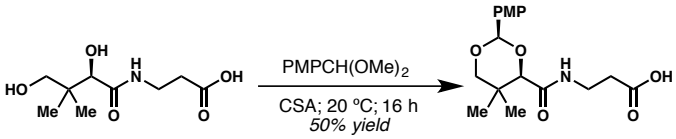

PMP-Protected Pantetheine Acid S1.

PMP-protection of *D*-pantothenic acid was performed as described by Burkart *et al*.[1] The spectroscopic data are consistent with previously reported data.[1-2]

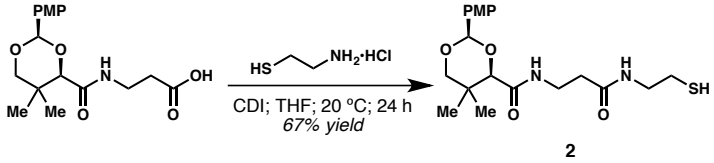

PMP-Protected Pantetheine Thiol 2.

CDI (72 mg, 0.45 mmol) was added in one aliquot to a stirring solution of PMP-protected acid **S1** (100 mg, 0.30 mmol) in 2 mL THF. Cysteamine·HCl (50 mg, 0.45 mmol) was added in one portion to the vigorously stirring reaction mixture 1 h after the complete dissolution of solids. After 24 h at ambient temperature, the solvent was removed *in vacuo* and the resultant viscous oil was suspended in CH_2Cl_2 (10 mL). The crude mixture was partitioned with an equivalent volume of sat. aq. NH_4Cl, and the aqueous layer was further extracted with CH_2Cl_2 (2 x 10 mL). The organic layers were combined, washed with brine (1 x 10 mL), dried over Na_2SO_4, filtered, and concentrated *in vacuo*. The amber residue was purified by flash column chromatography (SiO_2, 100% EtOAc + 1% v/v AcOH) to yield the desired thiol **2** (78 mg, 67%) as a pale yellow oil. ^1H NMR (500 MHz, $CDCl_3$) δ 7.40 (d, *J* = 8.4 Hz, 2 H), 7.01 (s, 1 H), 6.90 (d, *J* =

8.4 Hz, 2 H), 6.45 (s, 1 H), 5.44 (s, 1 H), 4.06 (s, 1 H), 3.80 (s, 3 H), 3.65 (q, *J* = 11.3 Hz, 2 H), 3.55–3.51 (m, 2 H), 3.39 (ddd, *J* = 26.5, 13.5, 6.7 Hz, 1 H), 3.33 (ddd, *J* = 26.0, 13.1, 6.1 Hz, 1 H), 2.57 (ap dd, *J* = 14.8, 7.3 Hz, 2 H), 2.41 (t, *J* = 6.5 Hz, 2 H), 1.33 (t, *J* = 8.3 Hz, 1 H), 1.07 (d, *J* = 7.6 Hz, 6 H); ^{13}C NMR (125 MHz, $CDCl_3$) δ 170.9, 169.5, 160.2, 130.0, 127.4, 113.7, 101.3, 83.7, 78.3, 55.3, 42.3, 35.9, 34.8, 33.0, 24.4, 21.8, 19.1; IR (thin film) 3318, 2957, 1660, 1615, 1519, 1461, 1391, 1249, 1103, 1031, 832, 731 cm^{-1}; HRMS (ESI) *m* / *z* calcd for $C_{19}H_{28}N_2O_5SNa$ [M + Na]$^+$ 419.1617, found 419.1630.

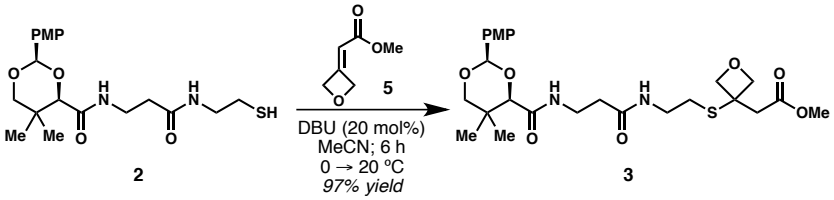

PMP-Protected Pantetheine Ester 3.

To a solution of PMP-protected thiol **2** (421 mg, 1.06 mmol) in 4 mL MeCN at 0 ºC was added methyl enoate **5** (150 mg, 1.2 mmol) in 2 mL MeCN. The reaction mixture was sparged for 5 min via the passage of Ar through the solution. Upon removing the sparging needle, DBU (30 μL, 0.19 mmol) was added in one aliquot. The pale yellow solution was warmed to ambient temperature and allowed to stir for 6 h. The reaction mixture was then concentrated to approximately 2 mL *in vacuo* and purified by flash column chromatography (SiO_2, 0 → 10% MeOH in EtOAC) to give the title compound (540 mg, 97% yield). ^{1}H NMR (500 MHz, $CDCl_3$) δ 7.42 (d, *J* = 8.5 Hz, 2 H), 7.03 (s, 1 H), 6.91 (d, *J* = 8.5 Hz, 2 H), 6.40 (s, 1 H), 5.45 (s, 1 H), 4.75 (dd, *J* = 4.7, 2.5 Hz, 2 H), 4.63 (dd, *J* = 6.9, 3.6 Hz, 2 H), 4.08 (s, 1 H), 3.82 (s, 3 H), 3.68 (s, 3 H and q, *J* = 11.9 Hz, 2 H), 3.59–3.48 (m, 2 H), 3.41 (ddd, *J* = 13.2, 6.6 Hz, 1 H), 3.37 (ddd, *J* = 26.4, 13.0, 6.2 Hz, 1 H), 2.98 (s, 2 H), 2.73 (t, *J* = 6.6 Hz, 2 H), 2.44 (t, *J* = 6.3 Hz, 2 H), 1.08 (d, *J* = 3.9 Hz, 6 H); ^{13}C NMR (125 MHz, $CDCl_3$) δ 171.0, 170.3, 169.5, 160.2, 130.2, 127.5, 113.7, 101.3, 83.8, 81.9, 78.5, 55.3, 51.9, 47.1, 42.4, 39.1, 35.9, 34.7, 33.1, 29.0, 21.8, 19.1; IR (thin film) 2952, 1735, 1663, 1519, 1249, 1103, 1030, 833 cm^{-1}; HRMS (ESI) *m* / *z* calcd for $C_{25}H_{36}N_2O_8SNa$ [M + Na]$^+$ 547.2090, found 547.2080.

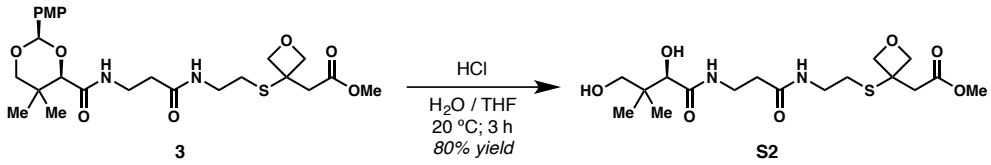

Pantetheine Methyl Ester S2.

Aqueous HCl (2 mL, 1 N) was added to a stirring solution of PMP-protected methyl ester **3** (100 mg, 0.19 mmol) in 2 mL THF. The solution was allowed to stir at ambient temperature until TLC indicated the complete consumption of starting material (3 h). Saturated aqueous $NaHCO_3$ (4 mL) was then added in one aliquot to neutralize the solution. The solvent was removed by passing N_2 gently over the vigorously stirring solution for 13 h. The beige salts were taken up in approximately 50 mL of 20% MeOH in CH_2Cl_2, sonicated to break up the solids, filtered, and concentrated *in vacuo* to yield the deprotected methyl ester **4** (80 mg, 80%) as a white solid. The crude methyl ester was used directly in the next step below without further purification. ^{1}H NMR (400 MHz, D_2O) δ 4.93 (d, *J* = 7.0 Hz, 2 H), 4.65 (d, *J* = 7.0 Hz, 2 H), 4.00 (s, 1 H), 3.73 (s, 3 H), 3.45–3.57 (m, 3 H), 3.35–3.43 (m, 3 H), 3.16 (s, 2 H), 2.82 (t, *J* = 6.4 Hz, 2 H), 2.50 (t, *J* = 5.4 Hz, 2 H), 0.93 (s, 3 H), 0.89 (s, 3 H); ^{13}C NMR (125 MHz, $CDCl_3$) δ 175.2, 174.1, 173.0, 82.2, 75.9, 68.5, 52.4, 46.7, 41.4, 39.0, 38.7, 35.6, 35.3, 28.2, 20.6, 19.2; HRMS (ES) *m* / *z* calcd for $C_{17}H_{30}N_2O_7SNa$ $[M + Na]^+$ 429.1671, found 429.1660.

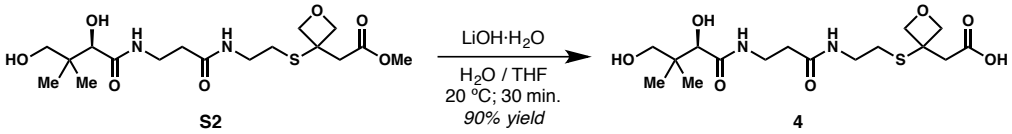

Pantetheine Carboxylic Acid 4.

Aqueous $LiOH{\cdot}H_2O$ (2 mL, 1 N) was added to a stirring solution of pantetheine methyl ester **S2** (80 mg, 0.20 mmol) in a 2:1 mixture of THF/H_2O (8 mL). The mixture was stirred at ambient temperature until TLC indicated complete consumption of starting material (30 min), upon which saturated aqueous $NaHCO_3$ (4 mL) was added in one aliquot. The crude reaction mixture was concentrated by gently passing N_2 over the vigorously stirring solution for 16 h. The white salts were suspended in approximately 30 mL of MeOH and sonicated to break up most of the solids. The slurry was then filtered and concentrated *in vacuo*, affording the title

compound (70 mg, 90% yield) as a white solid. No further purification was used prior to the next reaction (below). ^{1}H NMR (500 MHz, D_2O) δ 4.94 (d, *J* = 7.4 Hz, 2 H), 4.64 (d, *J* = 7.4 Hz, 2 H), 4.00 (s, 1 H), 3.55–3.51 (m, 3 H), 3.42 (t, *J* = 6.7 Hz, 2 H and d, *J* = 11.7 Hz, 1 H), 3.39 (s, 1 H), 2.85 (s, 2 H and t, *J* = 6.7 Hz, 2 H), 2.52 (t, *J* = 6.4 Hz, 2 H), 0.93 (s, 3 H), 0.90 (s, 3 H); ^{13}C NMR (125 MHz, CD_3OD) δ 178.1, 176.1, 173.8, 83.9, 77.2, 70.3, 49.9 46.9, 40.6, 40.4, 36.4, 36.3, 29.5, 21.4, 21.0; HRMS (ESI) *m* / *z* calcd for $C_{16}H_{28}N_2O_7SNa$ $[M + Na]^+$ 415.1515, found 415.1522.

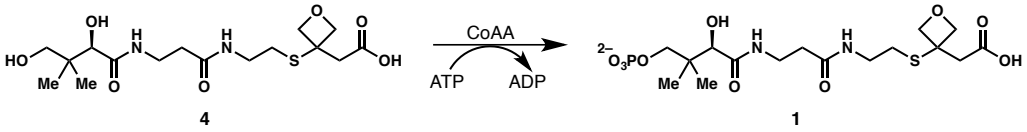

4 1

Malonate Mimic 1.

A buffer solution of potassium phosphate (25 mM, pH 7.5, 93 μL total volume), 1 M $MgCl_2$ (1 μL, 10 mM), 500 mM ATP·K_2 salt (1.6 μL, 8 mM), 57 μM CoAA (1.75 μL, 1 μM), 100 mM **4** in DMSO (2.5 μL, 2.5 mM) were added to an Eppendorf tube and homogenized with a vortex mixer. The reaction was incubated at 37 ºC for 90 min, upon which it was filtered using a Pierce™ Protein Concentrator (PES 3K WMCO). The solution was then injected into an HPLC column (Beckman Coulter™ Ultrasphere ODS, 5 μ particle size, 10 mm x 15 cm) and eluted with MeCN + 0.1% v/v formic acid in H_2O + 0.1% v/v (gradient elution: 5% → 95%). Fractions were analyzed using LRMS (ES) and the fractions containing product with the least ATP / ADP were pooled, concentrated under a stream of N_2, and used in the co-crystallographic studies without further purification. HRMS (ES) *m* / *z* calcd for $C_{16}H_{28}N_2O_{10}PS$ $[M + H]^-$ 471.1202, found 471.1208.

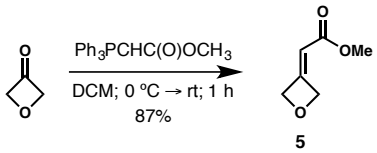

5

Methyl 2-(oxetan-3-ylidene)acetate (5).

Note: Methyl enoate ***5*** *was prepared by modification of the procedure of Wuitschik.*[3]

A solution of 3-oxetanone (200 mg, 2.8 mmol) in 2 mL CH_2Cl_2 was cooled to 0 ºC, upon which a solution of methyl (triphenylphosphoranylidene)acetate (1200 mg, 3.6 mmol) in 6 mL CH_2Cl_2 was transferred slowly via cannulation. The flask containing the Wittig reagent was rinsed with approximately 2 mL of CH_2Cl_2, which was cannulated into the reaction flask. After

30 min at 0 ºC, the flask was allowed to warm to ambient temperature. The pale yellow solution was allowed to stir for another 30 min, upon which it was poured onto a plug of silica gel and eluted with 1:1 EtOAc:hexanes. The volatiles were removed *in vacuo* yielding methyl enoate **5** (320 mg, 90% yield). ^{1}H NMR (500 MHz, $CDCl_3$) δ 5.64 (quin, *J* = 2.4 Hz, 1 H), 5.49 (ap dd, *J* = 6.9, 3.0 Hz, 2 H), 5.29 (ap dd, *J* = 7.0, 3.7 Hz, 2 H), 3.71 (s, 3 H); ^{13}C NMR (125 MHz, $CDCl_3$) δ 165.6, 159.1, 110.6, 81.0, 78.4, 51.4; IR (thin film) 2924, 2856, 2360, 1720, 1698, 1437, 1353, 1211, 1101, 956 cm^{-1}; HRMS (CI) *m* / *z* calcd for C_6H_9O $[M + H]^+$ 129.0552, found 129.0550.

IV. Expression and Purification of DpsC

A pET28 expression vector coding for 6xHis-tagged DpsC was transformed into *E. coli* BL21(DE3) by heatshocking at 42 °C for 45 seconds. The transformed cells were plated on an LB medium supplemented with 50 μg/mL kanamycin and incubated at 37 °C for 18 hours. Cells were transferred to a 10 mL starter culture supplemented with 50 μg/mL kanamycin and shaken at 250 rpm for 18 hours at 37 °C. 10 mL of the starter culture was transferred to 1 L of LB media supplemented with 50 μg/mL kanamycin. The cultures were shaken at 200 rpm at 37 °C until the OD_{600} reached 0.6; the expression was induced by addition of 1 mM IPTG, and the cultures were shaken for 18 hours at 18 °C. The cells were centrifuged for 10 minutes, resuspended in lysis buffer (50 mM Tris pH 8.0, 300 mM NaCl, 10 mM imidazole, 10% glycerol), and flash frozen in liquid nitrogen before storage at -80 °C.

The cells were lysed using a microfluidizer, and the lysate was centrifuged at 21,000 rcf for 1 hour to separate from cellular debris. The lysate was applied to a 5 mL HisTrap HP column (GE Healthcare) and eluted using an imidazole gradient via an Akta Purifier FPLC. The fractions were analyzed using SDS-PAGE, and the fractions containing DpsC were combined and concentrated to 5 mg/mL. The protein sample was further purified using a Superdex 200 column (GE Healthcare), and fractions were again analyzed using SDS-PAGE. The selected fractions containing DpsC were concentrated to 4 mg/mL and flash frozen in liquid nitrogen before storage at -80 °C.

V. Crystallization and Structure Solution of the Propionyl-DpsC-probe Complex

DpsC was crystallized in a solution containing 0.06 M $MgCl_2$, 0.6 M $CaCl_2$, 0.1 M imidazole pH 7.0, 0.1 M MES pH 6.7, 15% PEG 4000, and 30% Glycerol. The crystals were improved through multiple rounds of seeding using a Seed Bead (Hampton Research). The crystals were incubated in a 5 mM solution of propionyl-CoA prepared using mother liquor for 18 hours to form the propionyl-DpsC intermediate, transferred to a drop containing 5 mM **1** for 3 hours, and flash frozen in liquid nitrogen. The diffraction pattern of the crystals was measured at the Advanced Light Source using beamline 8.2.2. The diffraction images were processed using HKL2000[4]. The structure was solved by molecular replacement by Phaser using the *apo* DpsC structure (PDB:5TT4, submitted) as the search model[5]. The model was built by Coot and refined using the Phenix suite[6-8]. The statistics of data collection, processing and model building are listed in Table S1.

Molecular dynamics (MD) Simulations

The crystal structure of DpsC bound to oxetane-based probe **1** in this study was used for parameterization and setup of MD simulations. The same topology and coordinates of this structure were adopted for the simulation of DpsC with malonyl-PPT by mutating the oxetane-substituent *in silico* into a carbonyl group using the program Chimera. The Amber ff14SB force field[9-13] was used to parameterize the DpsC receptor. Two non-standard residues in DpsC were parameterized using RESP ESP charge Derive Server (R.E.D.S)[14-15]. Both malonate- and oxetane-based ligands were then parameterized using the general Amber force field (GAFF) and ff14SB forcefields[9-13].

Prior to minimization, complexes were neutralized with sixteen Na^+ counter-ions and solvated explicitly using a 10 Å buffer of TIP3P waters in a truncated octahedron box. Both systems underwent a two-step minimization using SANDER[9-13] to remove any steric clashes and overlaps. All hydrogen-containing bonds were constrained using the SHAKE algorithm[16]. DpsC-ligand complexes were then heated to 310K for 100-ps in the NVT ensemble, and equilibrated for 10-ns at 310K in the NPT ensemble. The accelerated CUDA version of PMEMD

was subsequently used to generate 100-ns production runs of all DpsC-ligand complexes in the NVT ensemble with 2-fs time steps.

For each of the two DpsC-ligand complexes – DpsC-malonyl-PPT and DpsC-**1**, three independent 100-ns trajectories were generated. A length of 100-ns for production runs is appropriate for both systems to converge at the physiological temperature. Backbone RMSD of DpsC complexes with respect to the first frame structure (Figure S5) demonstrates stability and convergence of the systems. Simulation conditions are listed in Table S2.

RMSD analysis of the two DpsC chains (chain A and chain B) in all six simulations revealed that RMSD of chain B converges to lower values (Figure S5). Given its higher stability, we then proceeded to compare the binding interactions between the malonate- and oxetane-based ligands in chain B of DpsC using the Molecular Mechanics Poissan-Boltzman Surface Area (MM/PBSA) module of Amber 16[17-22]. Specifically, the finite-difference Poisson Boltzmann method and the modern nonpolar solvation model were used in the solvation free energy calculation in MM/PBSA[23-28]. Considering the charged phosphopantetheine probes and DpsC residues, an internal protein dielectric constant of 20 was used in MM/PBSA calculations[21-22]. Both systems only differ with regards to a single substituent on the ligand – oxetane or carbonyl – thus *relative* binding affinity approximations are sufficient for analysis instead of *absolute* binding free energies (Table S3), which require more demanding conformational entropy calculations. Relative binding affinities were then calculated using the last 10-ns (frames 900 to 1000) of all three 100-ns production trajectories (Figure S). Convergence trend lines are provided in Figure S6, demonstrating the ΔG of both ligands converges after 6-ns. As listed in Table S3, the binding affinities of malonate- and oxetane-based probes are within one standard deviation of another, demonstrating similar binding affinities.

Using the CPPTRAJ module of Amber 16, we then conducted root-mean-square fluctuation (RMSF) analyses of backbone atoms (C, Cα, N, O) for all MD runs. The RMSF values provide overall movement of each residue from its mean position, revealing high-frequency motion of the protein. Loop regions and terminal sequences exhibit the highest degree of fluctuation. The average RMSF calculations of DpsC-malonate (Figure S7) and –oxetane (Figure S8) simulations are displayed. Further the average RMSF values are also visualized in the

context of the structures in Figure S9, rendered using the Chimera program. To determine long-time, overall motion of DpsC in response to either malonate- or oxetane-based ligands, the CPPTRAJ module of Amber 16 was employed once again to conduct Principal Component Analysis (PCA) and generate two movies[29]. PCA analysis consists of calculating a covariance matrix in which orthogonal vectors with the highest variance are selected as principal components (PCs). Using the first PC to generate movies of malonate- and oxetane-bound DpsC from DpsC-malonate simulation 1 and DpsC-oxetane simulation 5, we observe a general outward "breathing" motion exhibited by both complexes. Alpha helices 1-2 exhibit movement towards the ligand, and overall examination of PCA MD movies demonstrates minimal deviation between DpsC-malonate and DpsC-oxetane PCA movies. Figure S10 visualizes an alignment between the two snapshots closest to the mean structure (namely, with the lowest RMSD) of malonate and oxetane trajectories. Frame 337 of DpsC-malonate simulation 1 and frame 106 of DpsC-oxetane simulation 5 were chosen for alignment. The backbone (C, Cα, N) RMSD between the two mean structures is 0.716 Å, excluding the loop regions and the terminal regions. Overall, the computational analyses mentioned here demonstrate highly similar electronic, thermodynamic, and conformational influences propagated by malonyl-PPT and oxetane-based probe **1** in DpsC.

SI References

1. Clarke, K. M.; Mercer, A. C.; La Clair, J. J.; Burkart, M. D., *J Am Chem Soc* **2005,** *127* (32), 11234-5.
2. Shakya, G.; Rivera, H., Jr.; Lee, D. J.; Jaremko, M. J.; La Clair, J. J.; Fox, D. T.; Haushalter, R. W.; Schaub, A. J.; Bruegger, J.; Barajas, J. F.; White, A. R.; Kaur, P.; Gwozdziowski, E. R.; Wong, F.; Tsai, S. C.; Burkart, M. D., *J Am Chem Soc* **2014,** *136* (48), 16792-9.
3. Wuischik, G. Oxetanes in Drug Discovery. . ETH Zürich,, 2008.
4. Otwinowski, Z.; Minor, W., *Method Enzymol* **1997,** *276*, 307-326.
5. Mccoy, A. J.; Grosse-Kunstleve, R. W.; Adams, P. D.; Winn, M. D.; Storoni, L. C.; Read, R. J., *J Appl Crystallogr* **2007,** *40*, 658-674.
6. Emsley, P.; Cowtan, K., *Acta Crystallogr D* **2004,** *60*, 2126-2132.
7. Terwilliger, T. C.; Grosse-Kunstleve, R. W.; Afonine, P. V.; Moriarty, N. W.; Zwart, P. H.; Hung, L. W.; Read, R. J.; Adams, P. D., *Acta Crystallogr D* **2008,** *64*, 61-69.
8. Afonine, P. V.; Grosse-Kunstleve, R. W.; Echols, N.; Headd, J. J.; Moriarty, N. W.; Mustyakimov, M.; Terwilliger, T. C.; Urzhumtsev, A.; Zwart, P. H.; Adams, P. D., *Acta Crystallogr D* **2012,** *68*, 352-367.
9. Case, D. A., Darden, T., Cheatham, T.E., III, Adrian Roitberg, C.S., Wang, J., Duke, R.E., Luo, R., Roe, D.R., Walker, R.C., Legrand, S., et al. (2014b), **Amber 14 Reference Manual (University of California)**.
10. Gotz, A. W.; Williamson, M. J.; Xu, D.; Poole, D.; Le Grand, S.; Walker, R. C., *J Chem Theory Comput* **2012,** *8* (5), 1542-1555.
11. Wang, J.; Wang, W.; Kollman, P. A.; Case, D. A., *J Mol Graph Model* **2006,** *25* (2), 247-60.
12. Wang, J.; Wolf, R. M.; Caldwell, J. W.; Kollman, P. A.; Case, D. A., *J Comput Chem* **2004,** *25* (9), 1157-74.
13. Wickstrom, L.; Okur, A.; Simmerling, C., *Biophys J* **2009,** *97* (3), 853-6.
14. Dupradeau, F. Y.; Pigache, A.; Zaffran, T.; Savineau, C.; Lelong, R.; Grivel, N.; Lelong, D.; Rosanski, W.; Cieplak, P., *Phys Chem Chem Phys* **2010,** *12* (28), 7821-39.
15. Vanquelef, E.; Simon, S.; Marquant, G.; Garcia, E.; Klimerak, G.; Delepine, J. C.; Cieplak, P.; Dupradeau, F. Y., *Nucleic Acids Res* **2011,** *39* (Web Server issue), W511-7.
16. Ryckaert, J. P. C., G.; Berendsen, H. J. C., *Journal of Computational Physics* **1977,** *23*, 327-341.
17. Gohlke, H.; Case, D. A., *J Comput Chem* **2004,** *25* (2), 238-50.
18. Kollman, P. A.; Massova, I.; Reyes, C.; Kuhn, B.; Huo, S.; Chong, L.; Lee, M.; Lee, T.; Duan, Y.; Wang, W.; Donini, O.; Cieplak, P.; Srinivasan, J.; Case, D. A.; Cheatham, T. E., 3rd, *Acc Chem Res* **2000,** *33* (12), 889-97.
19. Miller, B. R., 3rd; McGee, T. D., Jr.; Swails, J. M.; Homeyer, N.; Gohlke, H.; Roitberg, A. E., *J Chem Theory Comput* **2012,** *8* (9), 3314-21.
20. Srinivasan, J. C., T. E.; Cieplak, P.; Kollman, P. A.; Case, D. A., *Journal of the American Chemical Society* **1998,** (120), 9401-9409.
21. Wang, C.; Nguyen, P. H.; Pham, K.; Huynh, D.; Le, T. B.; Wang, H.; Ren, P.; Luo, R., *J Comput Chem* **2016,** *37* (27), 2436-46.
22. Yang, T. Y. W., J. C.; Yan, C. L.; Wang, Y. F.; Luo, R.; Gonzales, M. B.; Dalby, K. N.; Ren, P. Y., *Proteins-Structure Function and Bioinformatics* **2011,** *79*, 1940-1951.
23. Wang, J.; Cai, Q.; Li, Z.-L.; Zhao, H.-K.; Luo, R., *Chemical Physics Letters* **2009,** *468* (4-6), 112-118.
24. Wang, J.; Luo, R., *Journal of Computational Chemistry* **2010,** *31* (8), 1689-1698.
25. Cai, Q.; Hsieh, M.-J.; Wang, J.; Luo, R., *Journal of Chemical Theory and Computation* **2010,** *6* (1), 203-211.
26. Wang, J.; Cai, Q.; Xiang, Y.; Luo, R., *Journal of Chemical Theory and Computation* **2012,** *8* (8), 2741-2751.
27. Botello-Smith, W. M.; Luo, R., *J Chem Inf Model* **2015,** *55* (10), 2187-99.

28. Tan, C.; Tan, Y.-H.; Luo, R., *Journal of Physical Chemistry B* **2007,** *111* (42), 12263-12274.
29. Galindo-Murillo, R.; Roe, D. R.; Cheatham, T. E., 3rd, *Biochim Biophys Acta* **2015,** *1850* (5), 1041-58.
30. de Beer, T. A.; Berka, K.; Thornton, J. M.; Laskowski, R. A., *Nucleic Acids Res* **2014,** *42* (Database issue), D292-6.
31. Laskowski, R. A., *Nucleic Acids Res* **2001,** *29* (1), 221-2.
32. Laskowski, R. A.; Hutchinson, E. G.; Michie, A. D.; Wallace, A. C.; Jones, M. L.; Thornton, J. M., *Trends Biochem Sci* **1997,** *22* (12), 488-90.

SI Tables

Table S1. Statistics of Data Collection, Processing and Refinement

	prop-DpsC + **1**
Data collection	
Wavelength (Å)	1.0
Total reflections	85634 (7822)
Unique reflections	43341 (4164)
Space group	P 6_5 2 2
Cell dimensions	
a, *b*, *c* (Å)	91.6, 91.6, 316.1
α, β, γ (°)	90, 90, 120
Resolution (Å)	70.9 – 2.15
R_{merge}	0.021 (0.134)
R_{meas}	0.030 (0.190)
$I/\sigma(I)$	16.26 (4.26)
$CC_{1/2}$	0.999 (0.978)
CC*	1.0 (0.994)
Completeness (%)	99 (95)
Redundancy	2.0 (1.9)
Wilson B-factor	35.15
Refinement	
Resolution (Å)	70.9 – 2.15
No. reflections	43233 (4160)
R_{work}	0.179
R_{free}	0.209
No. atoms	
Protein	5083
Ligands	60
B factors	
Protein	39.56
Ligands	95.06
Water	44.86
Ramachandran	

Table S2. DpsC & Ligand Simulation Conditions

Simulation Number	System	Temperature (K)	Time (ns)	Traj. Num.	Ions	Waters
1	DpsC & malonate-based **1**	310	100	1	16 Na^+	14,767
2	DpsC & malonate-based **1**	310	100	1	16 Na^+	14,767
3	DpsC & malonate-based **1**	310	100	1	16 Na^+	14,767
4	DpsC & oxetane-based **1**	310	100	1	16 Na^+	14,769
5	DpsC & oxetane-based **1**	310	100	1	16 Na^+	14,769
6	DpsC & oxetane-based **1**	310	100	1	16 Na^+	14,769

Table S3. MM/PBSA-derived Δ*G* Relative Binding Free Energy Approximations (kcal/mol)

Simulation Number	DpsC Chain & Ligand	Δ*G*	Standard Deviation	Standard Error
1	DpsC Chain B & malonate-based **1**	-16.83	4.54	0.144
2	DpsC Chain B & malonate-based **1**	-16.00	4.14	0.131
3	DpsC Chain B & malonate-based **1**	-13.43	4.32	0.137
4	DpsC Chain B & oxetane-based **1**	-15.36	3.68	0.117
5	DpsC Chain B & oxetane-based **1**	-15.11	4.03	0.128
6	DpsC Chain B & oxetane-based **1**	-15.45	3.70	0.117

SI Figures

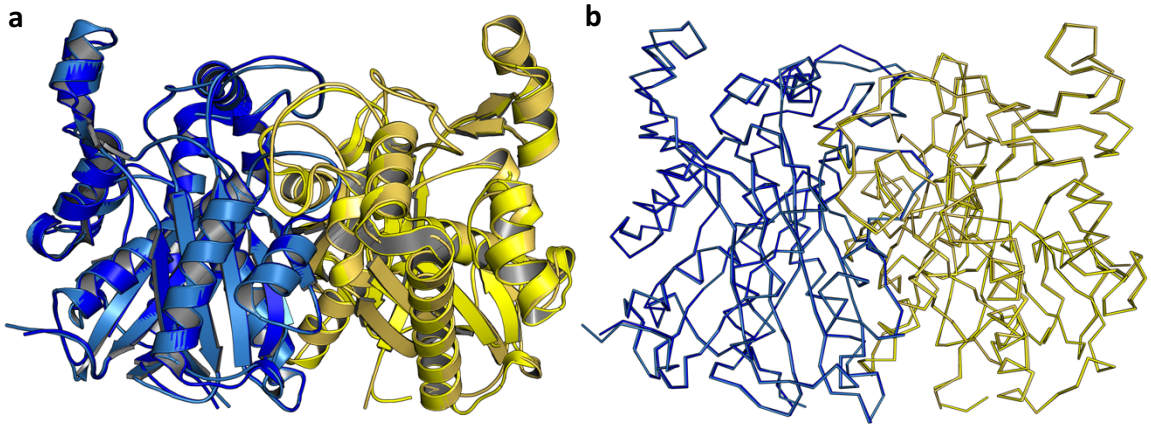

Figure S1. Ligand-free and ligand-bound structural comparison. **a**, the ligand-free structure of prop-DpsC (dark blue and bright yellow) is overlaid with the ligand-bound structure (light blue and pale yellow) in cartoon representation. **b**, the ligand-free structure of prop-DpsC (dark blue and bright yellow) is overlaid with the ligand-bound structure (light blue and pale yellow) in ribbon representation.

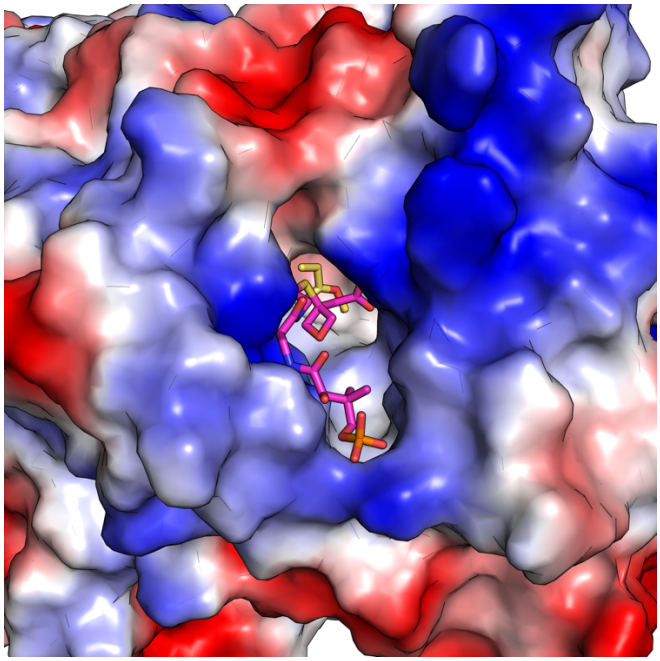

Figure S2. DpsC active site pocket. The surface of DpsC is represented as surface electrostatics. **1** is shown in magenta sticks, and the propionylated S118 sidechain is shown in yellow sticks.

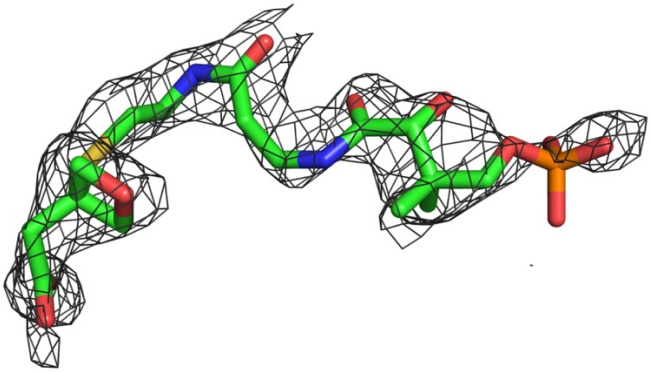

Figure S3. SA-Omit $|2F_o\text{-}F_c|$ map for **1** contoured at 0.8 sigma.

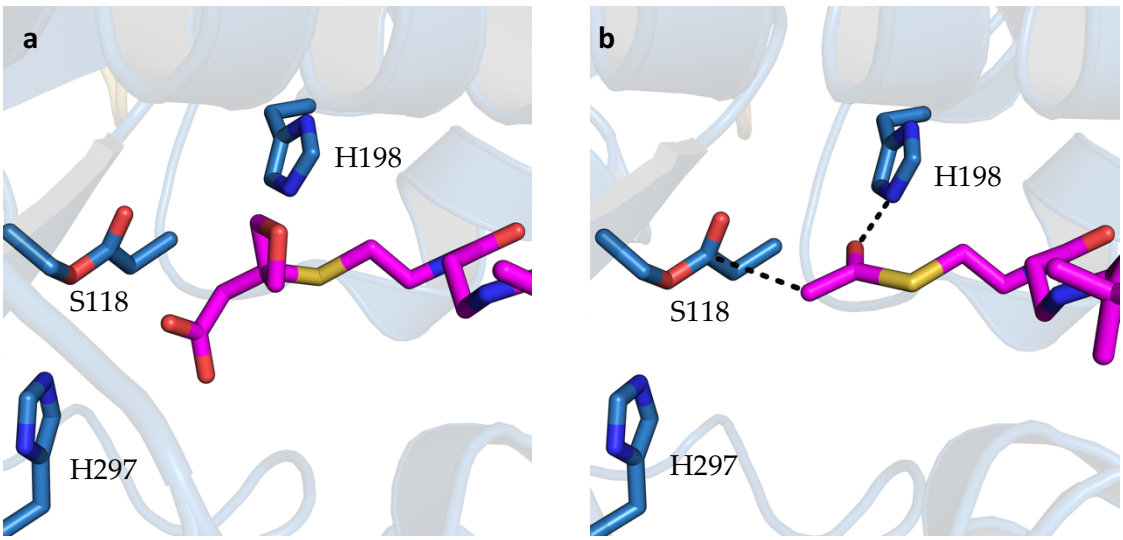

Figure S4. Proposed DpsC oxyanion hole. **a**, crystal structure of prop-DpsC with **1**, showing the putative oxyanion hole residue H198. **b**, a proposed model showing a post-decarboxylation substrate that has rotated to interact with H198.

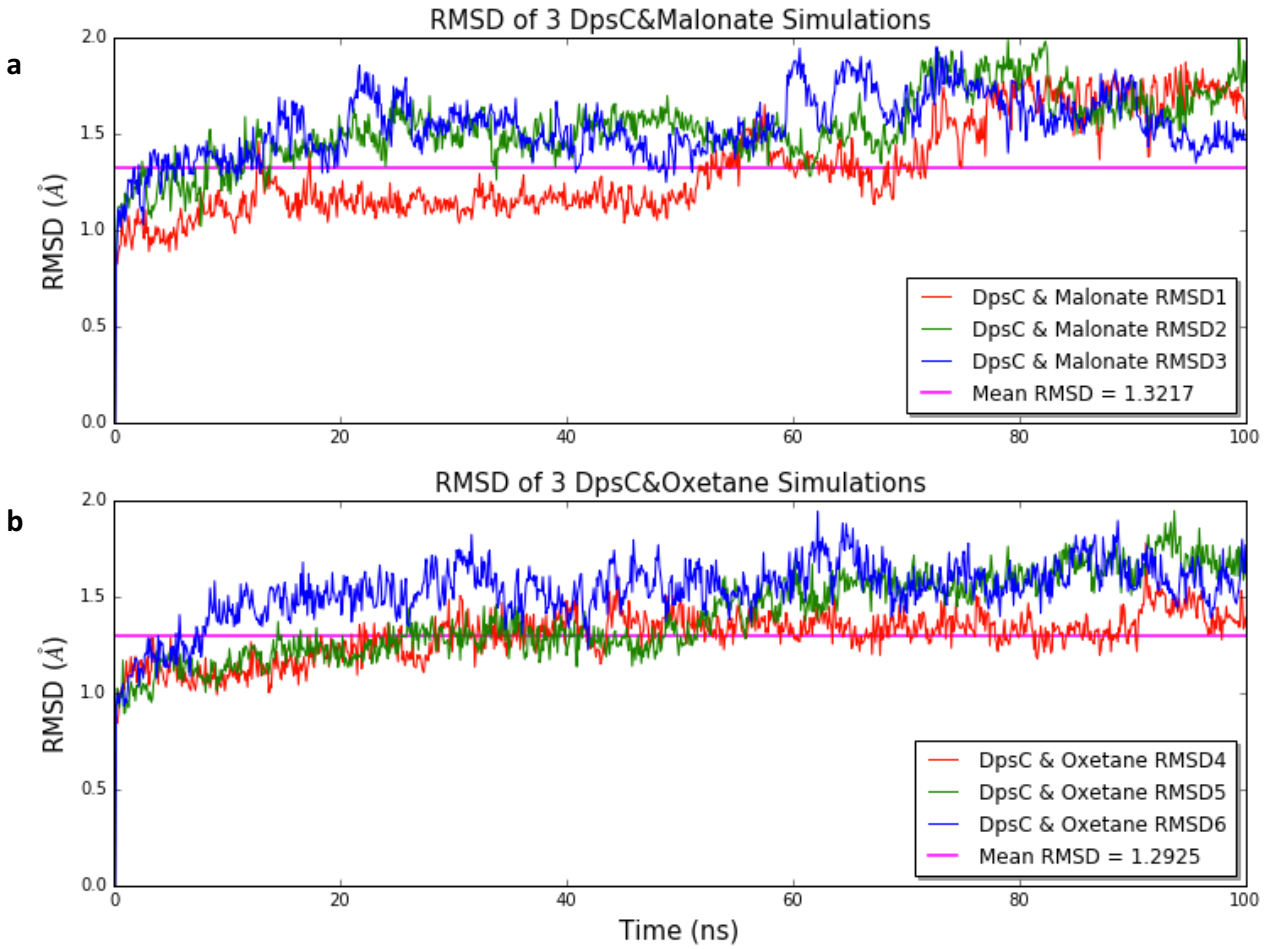

Figure S5. Backbone (C, Cα, N, O) RMSD of 100-ns, DpsC-malonate simulations 1-3 and DpsC-oxetane simulations 4-6. **a**, all DpsC-malonate simulations converge within 100-ns, averaging to 1.322 Å. **b**, all DpsC-oxetane simulations converge within 100-ns, averaging to 1.292 Å.

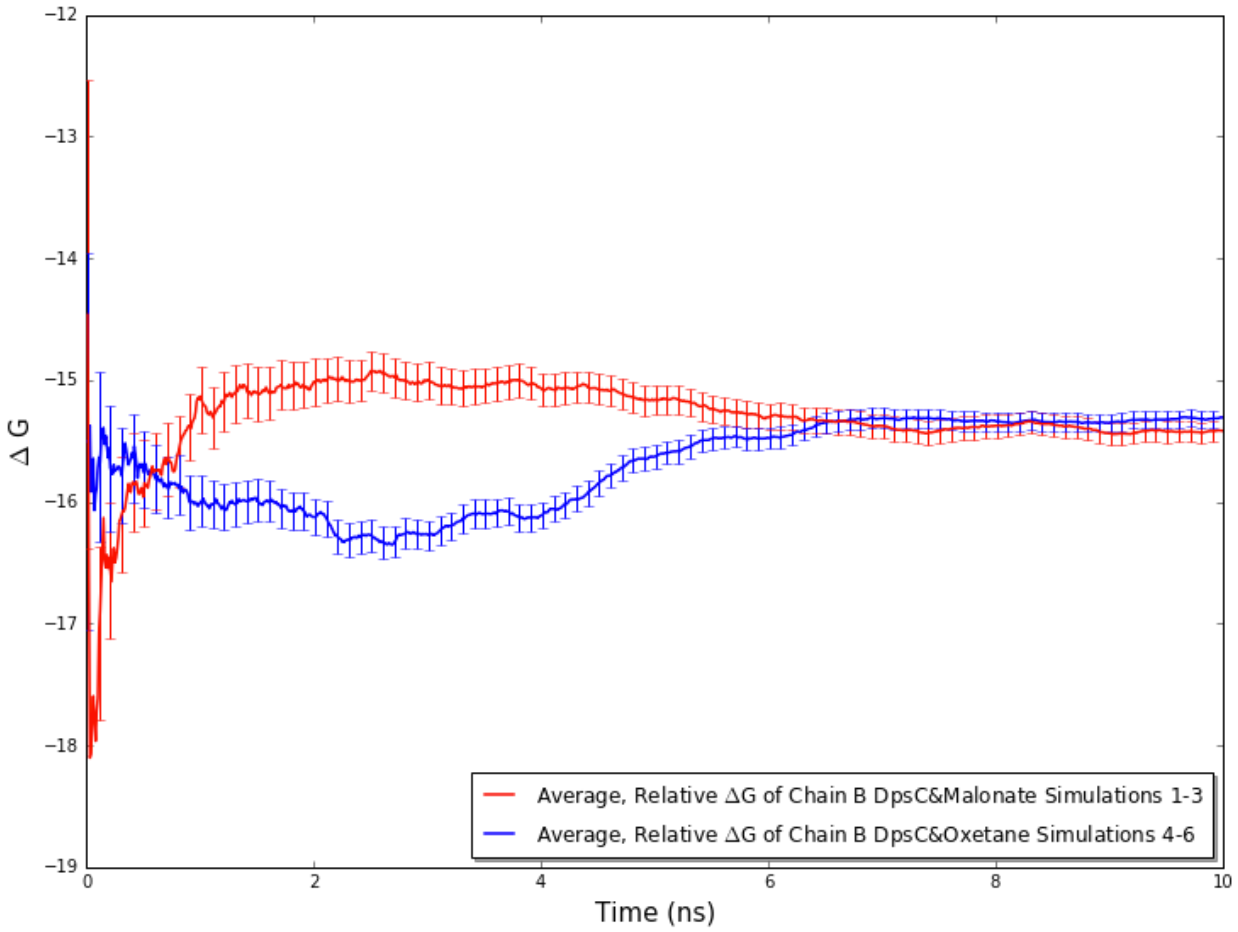

Figure S6. Convergence trend lines of average ΔG binding energy calculations of DpsC-malonate simulations 1-3 and DpsC-oxetane simulations 4-6. The malonate-bound average ΔG converges to -44.50 kcal/mol after 7 ns, and oxetane-bound average ΔG converges to -45.80 kcal/mol after 7 ns.

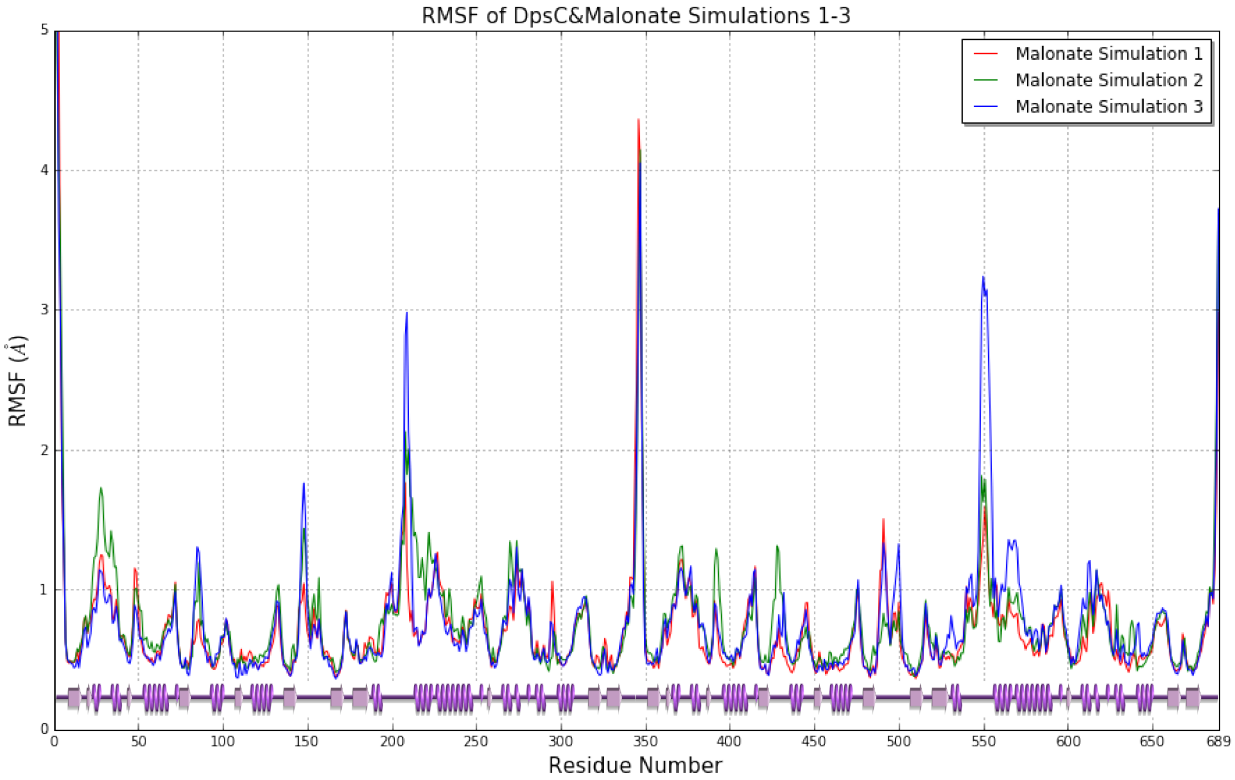

Figure S7. Heavy-atom (C, Cα, N, O) RMSF of all DpsC-malonate simulations. Secondary structure is depicted using PDBsum-generated imaging adjacent to the x-axis[30-32].

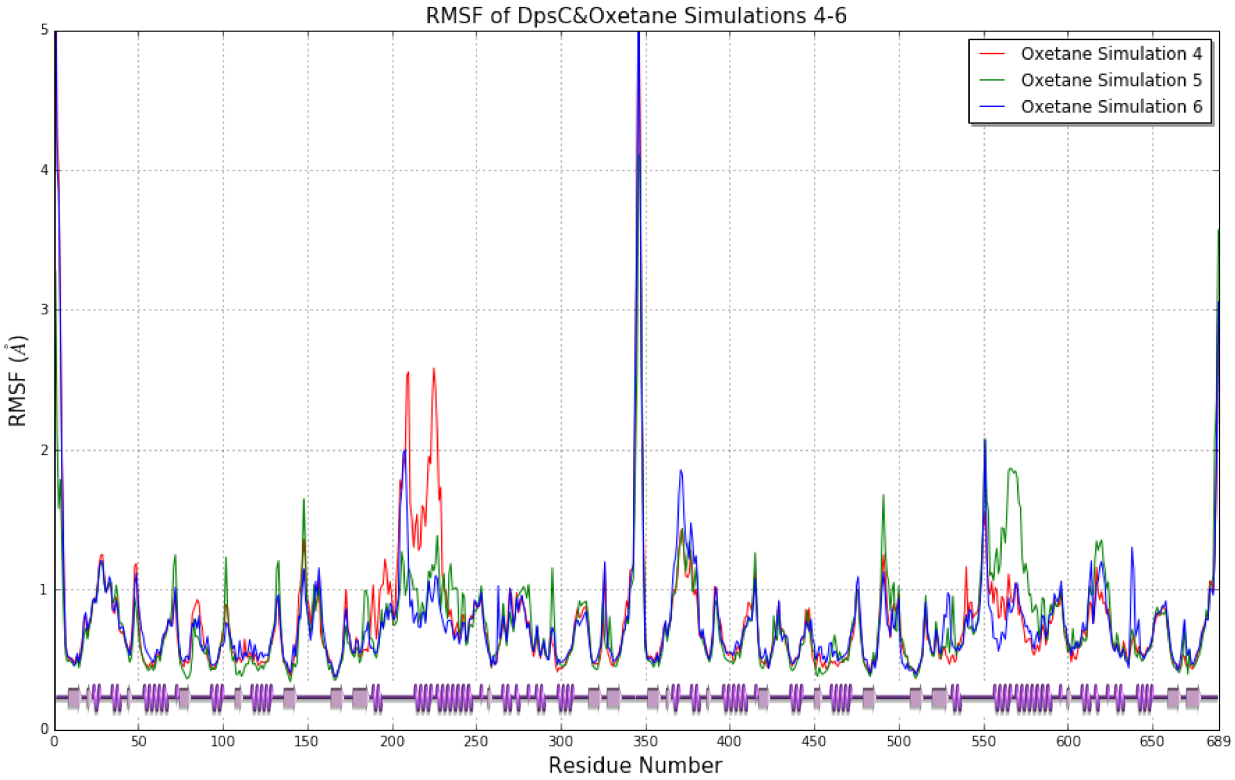

Figure S8. Heavy-atom (C, Cα, N, O) RMSF of all DpsC-oxetane simulations. Secondary structure is depicted using PDBsum-generated imaging adjacent to the x-axis[30-32].

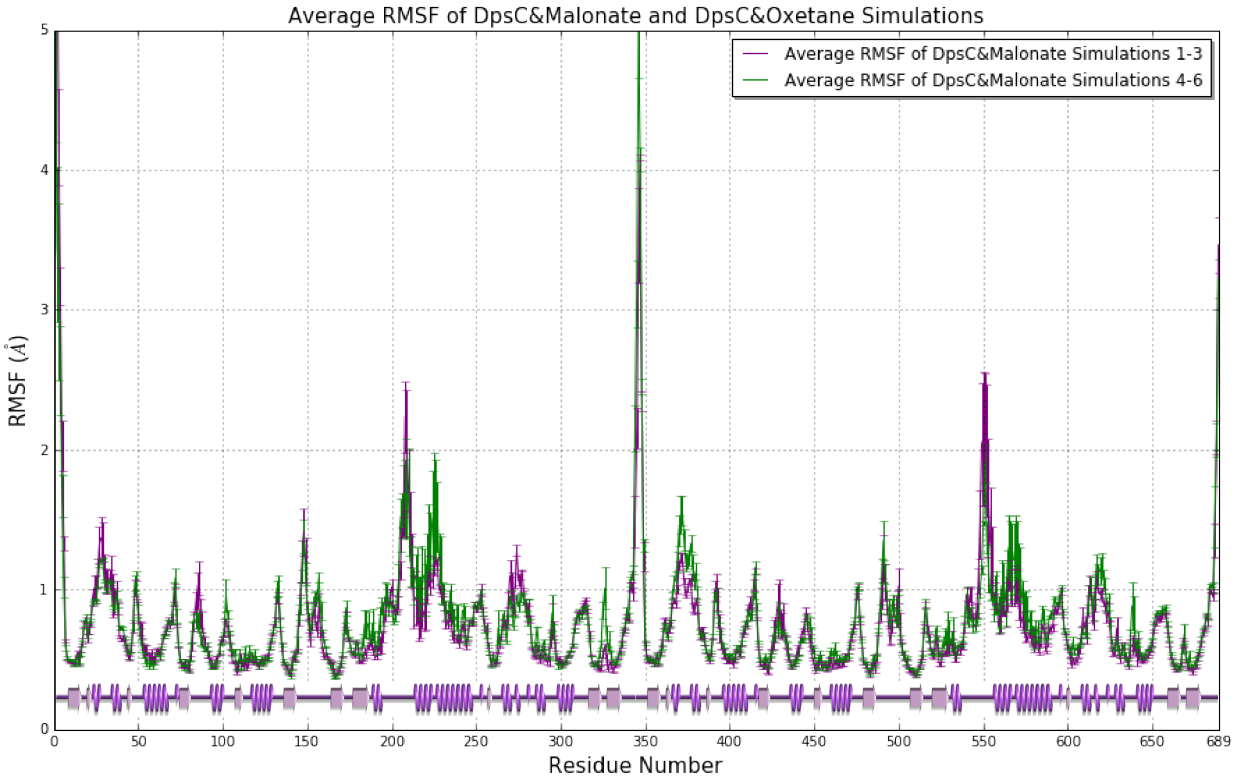

Figure S9. Average backbone (C, Cα, N, O) RMSF of all DpsC-malonate and DpsC-oxetane simulations. Secondary structure is depicted using PDBsum-generated imaging adjacent to the x-axis[30-32].

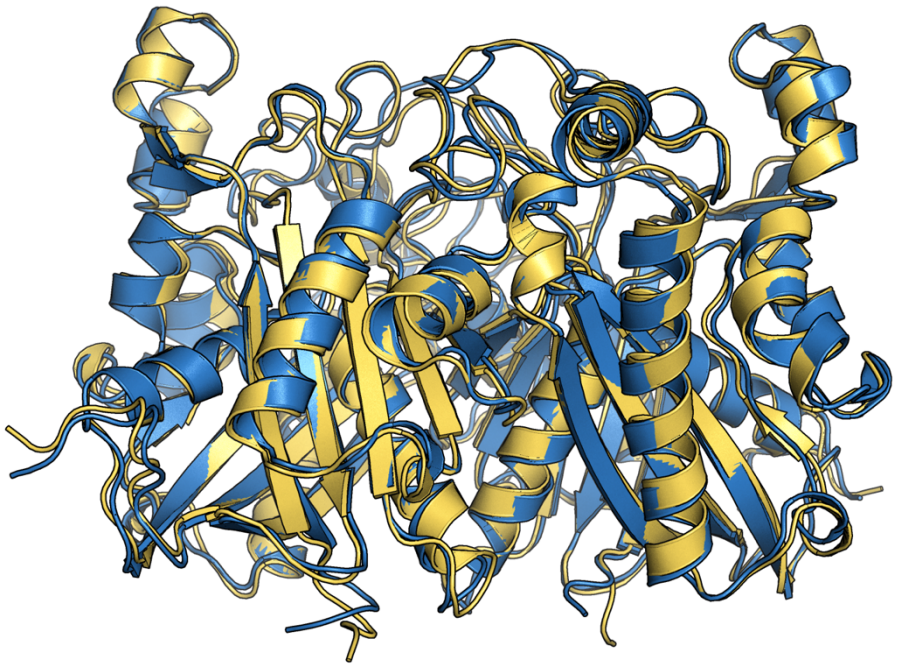

Figure S10. Alignment of mean structures from DpsC-malonate simulations (yellow) and DpsC-oxetane simulations (blue). Backbone RMSD is 0.716Å after alignment.

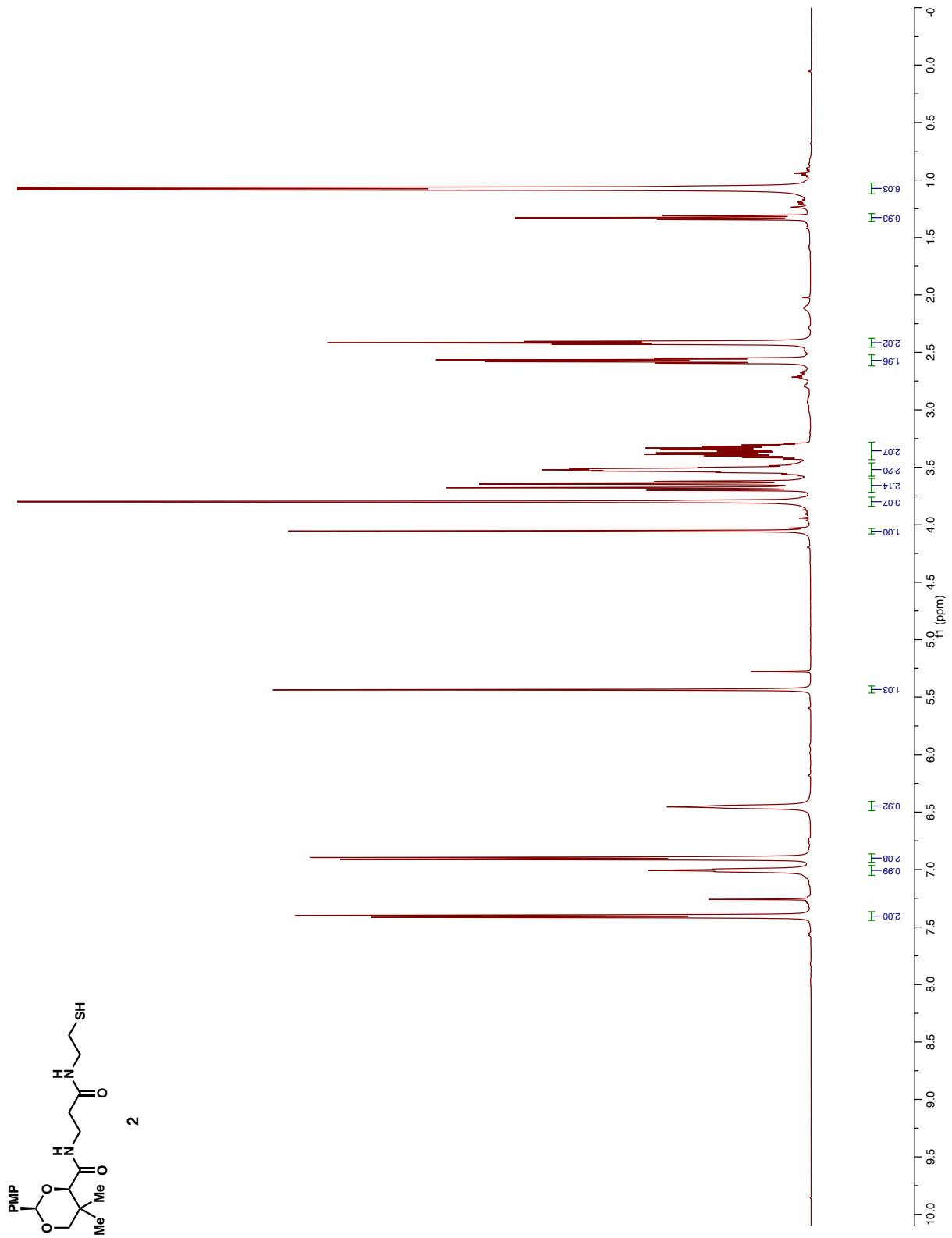
PMP
O
O
Me
Me
O
H
N
O
H
N
SH
2
6.03
0.93
2.02
1.96
2.07
2.20
2.14
3.07
1.00
1.03
0.92
0.99
2.08
2.00
f1 (ppm)

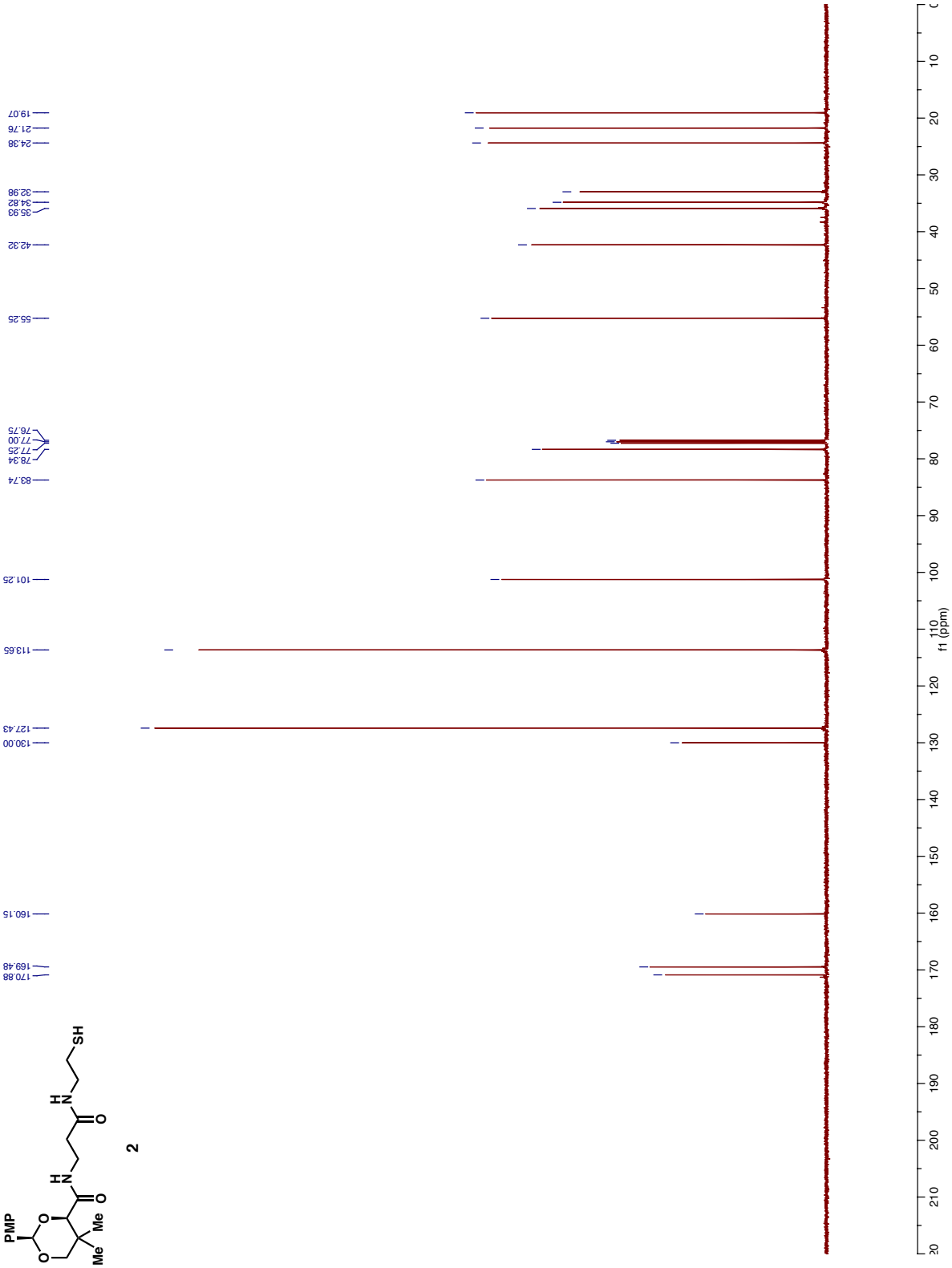
19.07
21.76
24.38
32.98
34.82
35.93
42.32
55.25
76.75
77.00
77.25
78.34
83.74
101.25
113.65
127.43
130.00
160.15
169.48
170.88
PMP
Me
Me
O
O
O
O
H
N
H
N
O
SH
2
f1 (ppm)

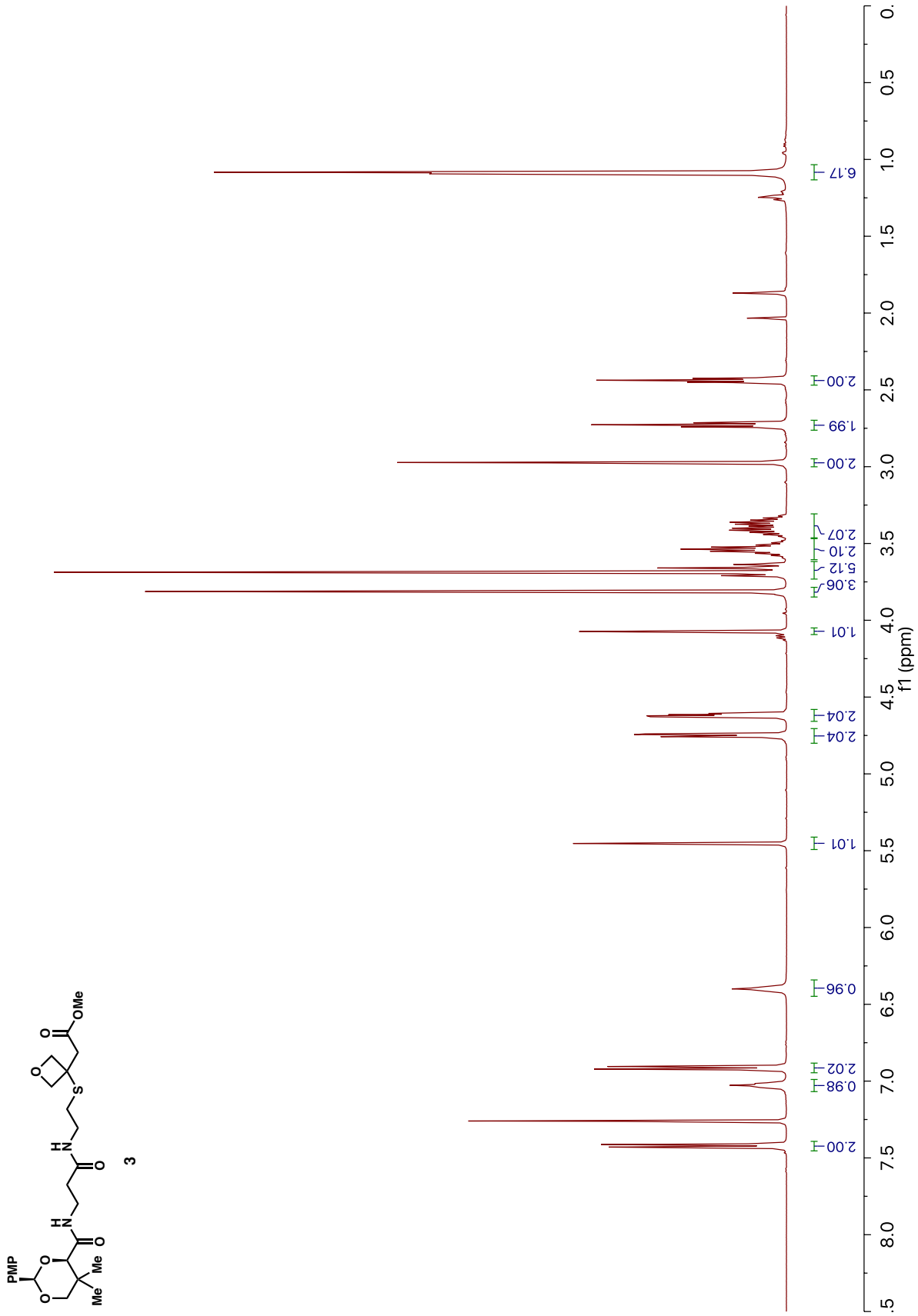
PMP
Me
Me
O
H
N
O
H
N
O
S
O
O
OMe
3
6.17
2.00
1.99
2.00
2.07
2.10
5.12
3.06
1.01
2.04
2.04
1.01
0.96
2.02
0.98
2.00
f1 (ppm)

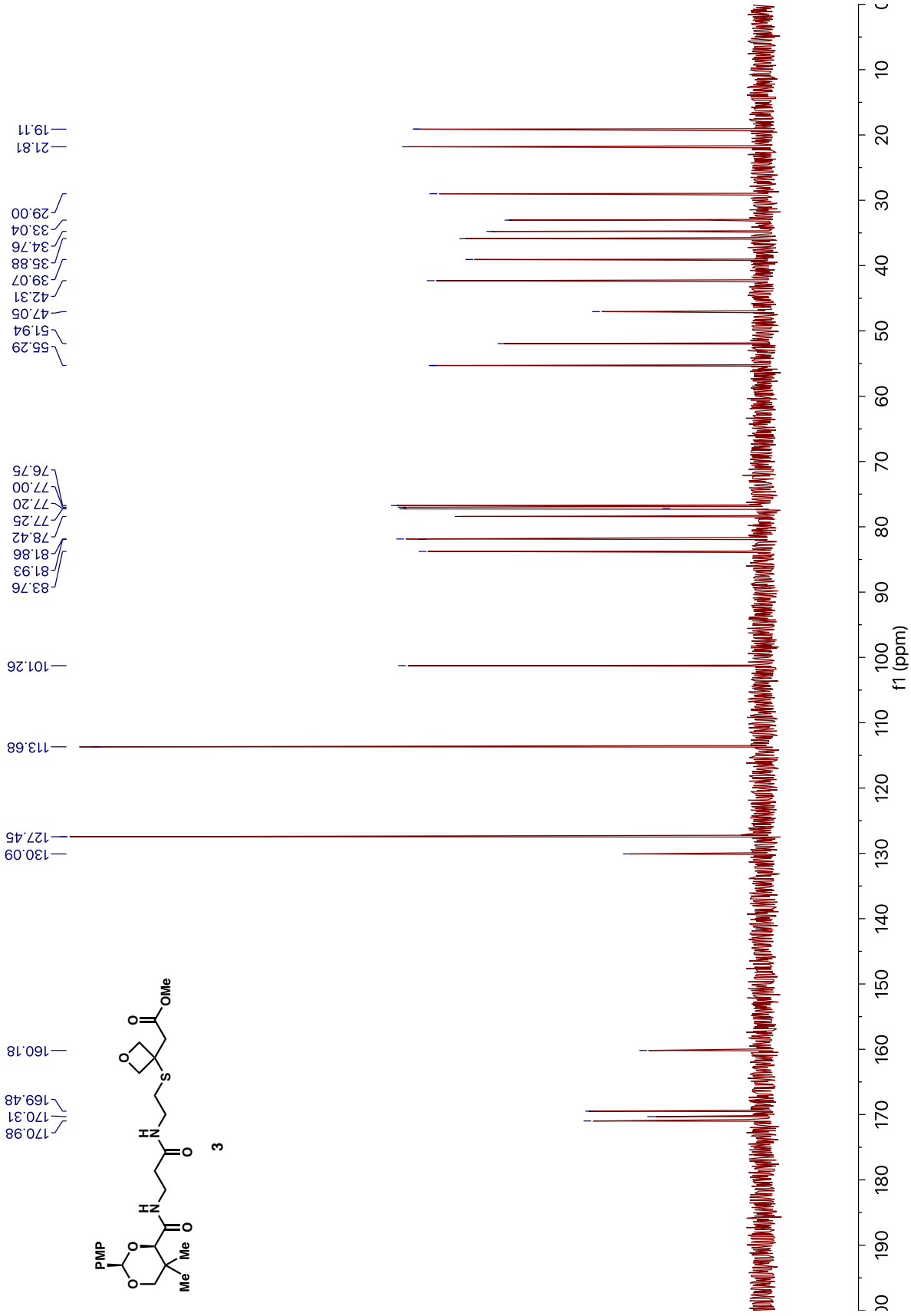
170.98
170.31
169.48
160.18
130.09
127.45
113.68
101.26
83.76
81.93
81.86
78.42
77.25
77.20
77.00
76.75
55.29
51.94
47.05
42.31
39.07
35.88
34.76
33.04
29.00
21.81
19.11
PMP
Me
Me
O
N
H
O
N
H
O
S
O
O
OMe
3
f1 (ppm)

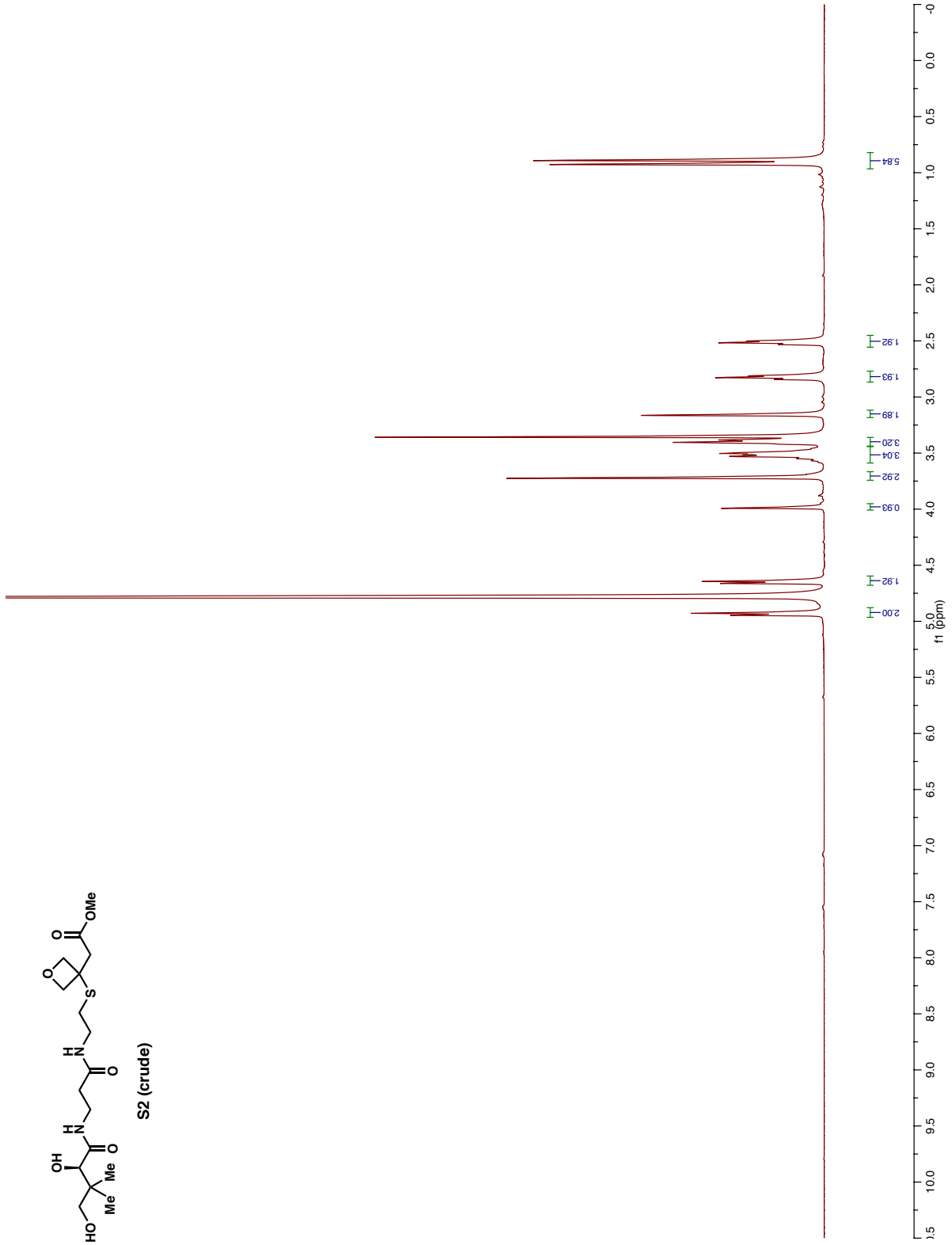
S2 (crude)
5.84
1.92
1.93
1.89
3.20
3.04
2.92
0.93
1.92
2.00
f1 (ppm)

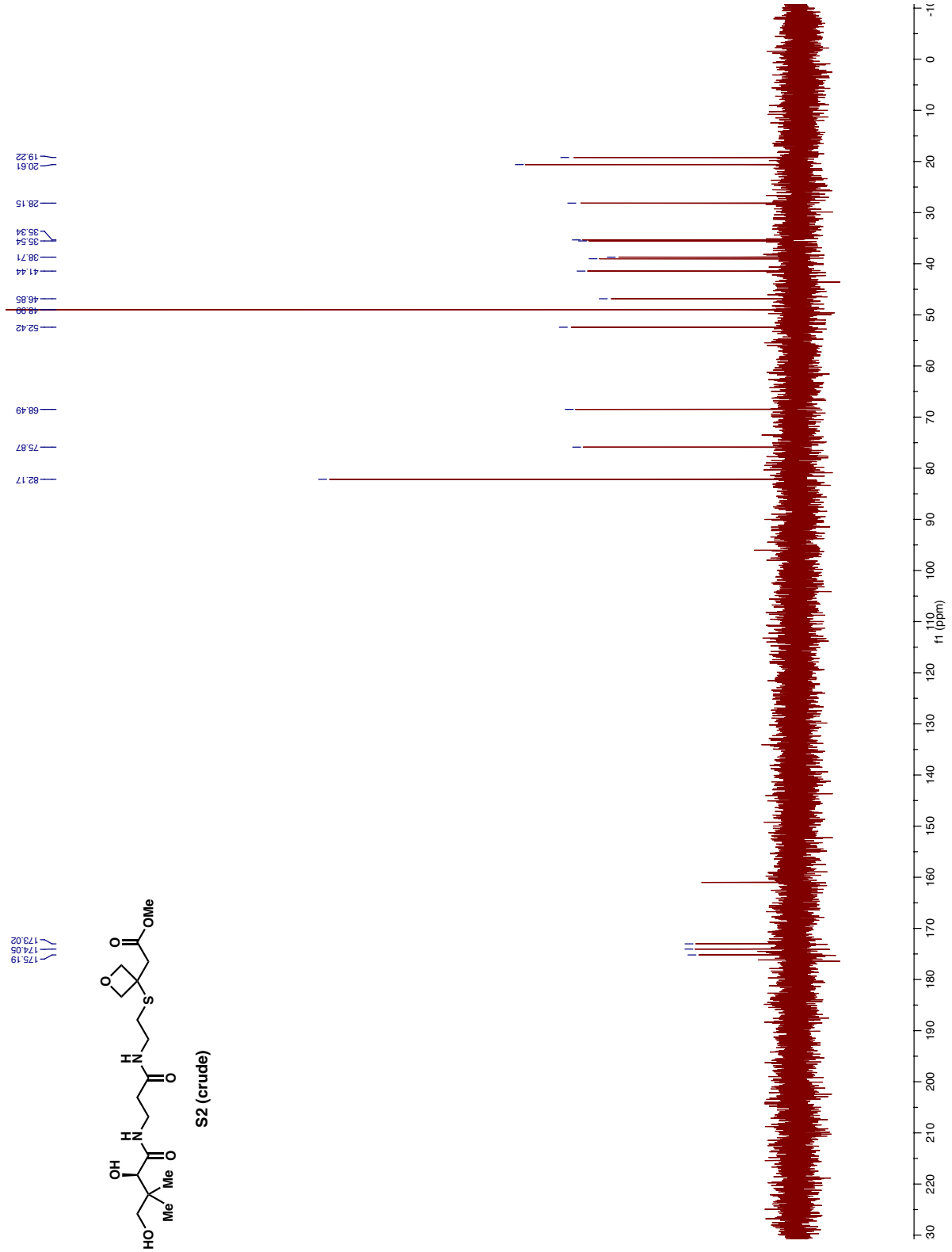
19.22
20.61
28.15
35.34
35.54
38.71
41.44
46.85
48.80
52.42
68.49
75.87
82.17
173.02
174.05
175.19
OMe
O
S
N
H
O
N
H
O
OH
Me
Me
HO
S2 (crude)
f1 (ppm)

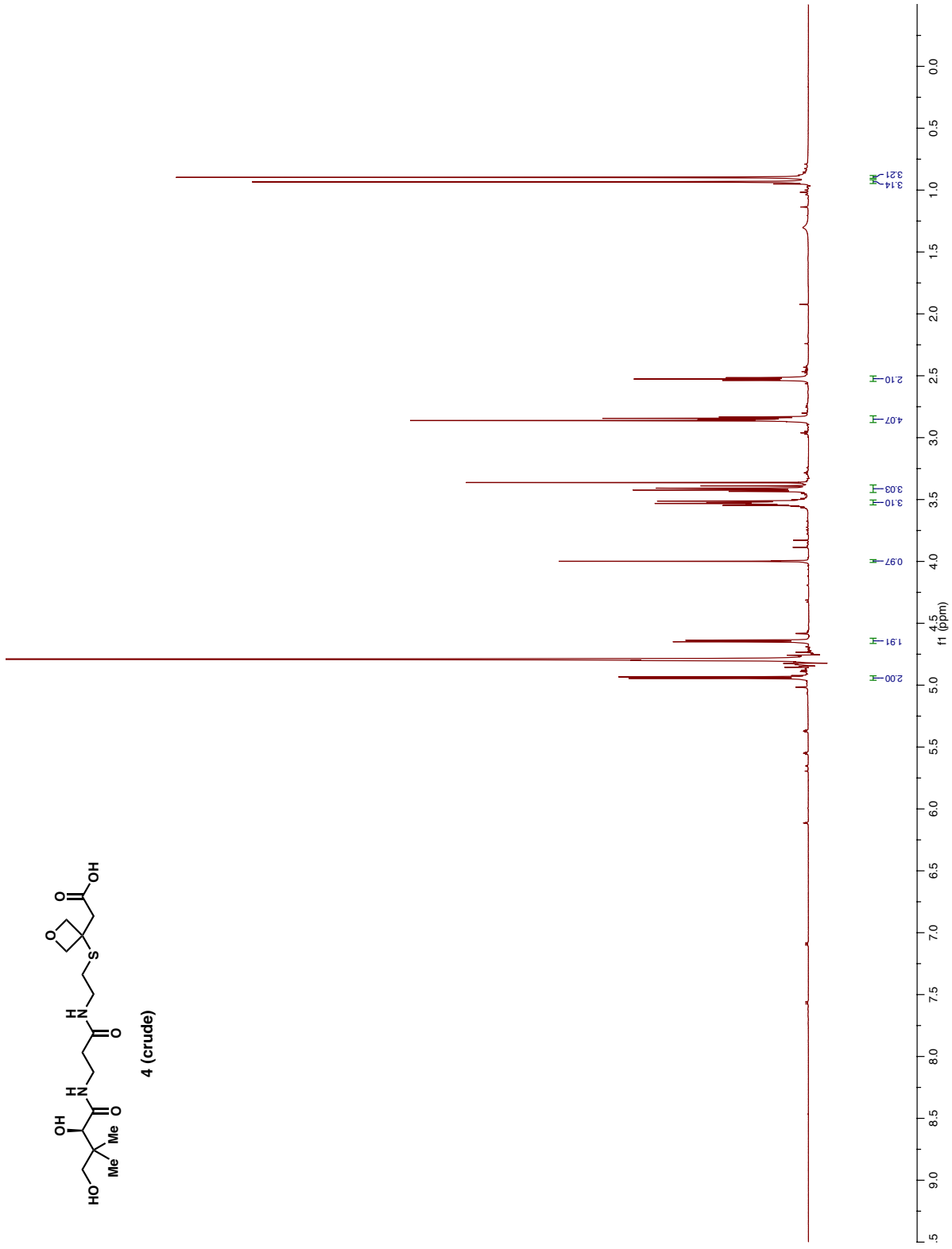
4 (crude)
3.21
3.14
2.10
4.07
3.03
3.10
0.97
1.91
2.00
f1 (ppm)

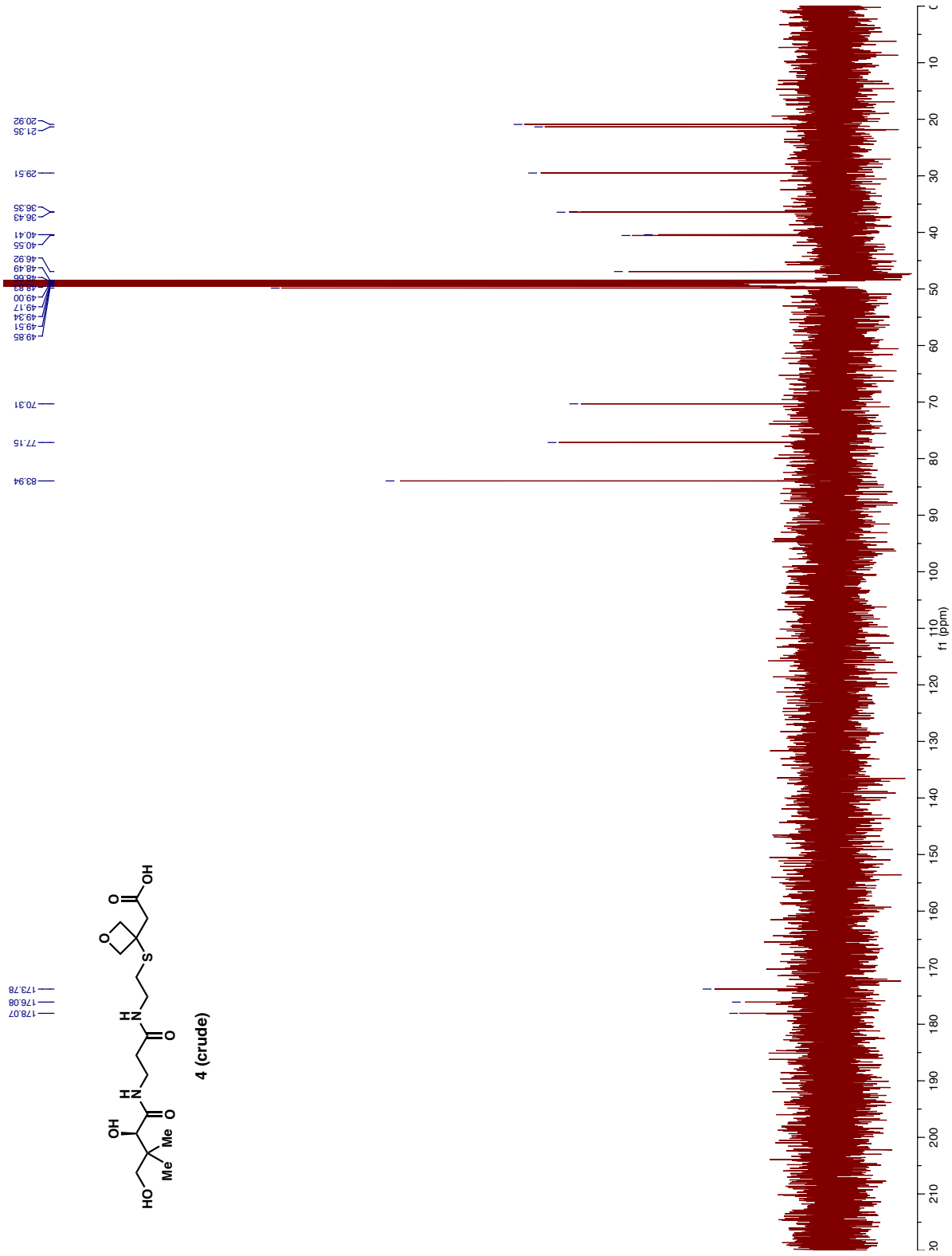
20.92
21.35
29.51
36.35
36.43
40.41
40.55
46.92
48.49
48.66
48.83
49.00
49.17
49.34
49.51
49.85
70.31
77.15
83.94
173.78
176.08
178.07
4 (crude)
f1 (ppm)

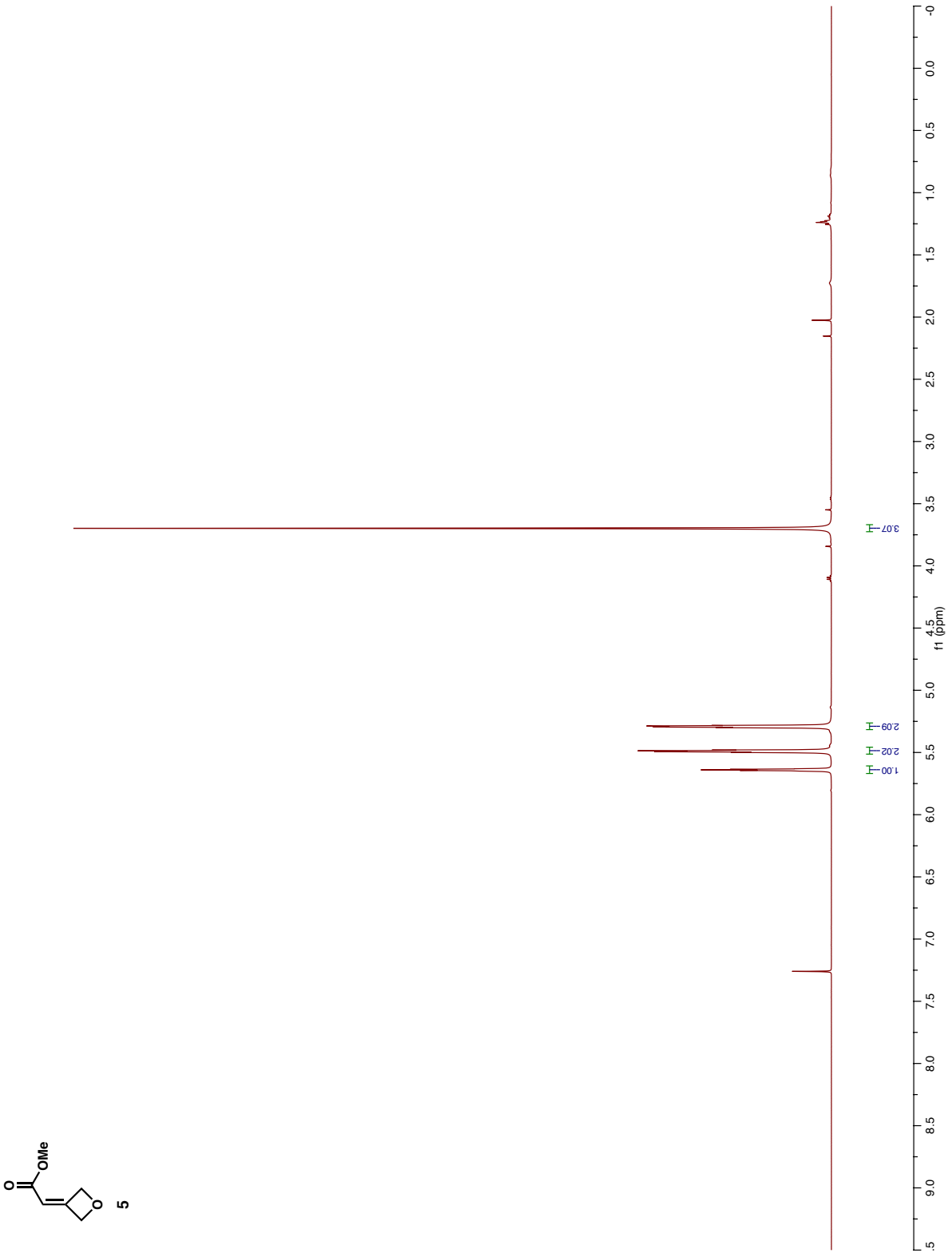
OMe
O
O
5
3.07
2.09
2.02
1.00
f1 (ppm)

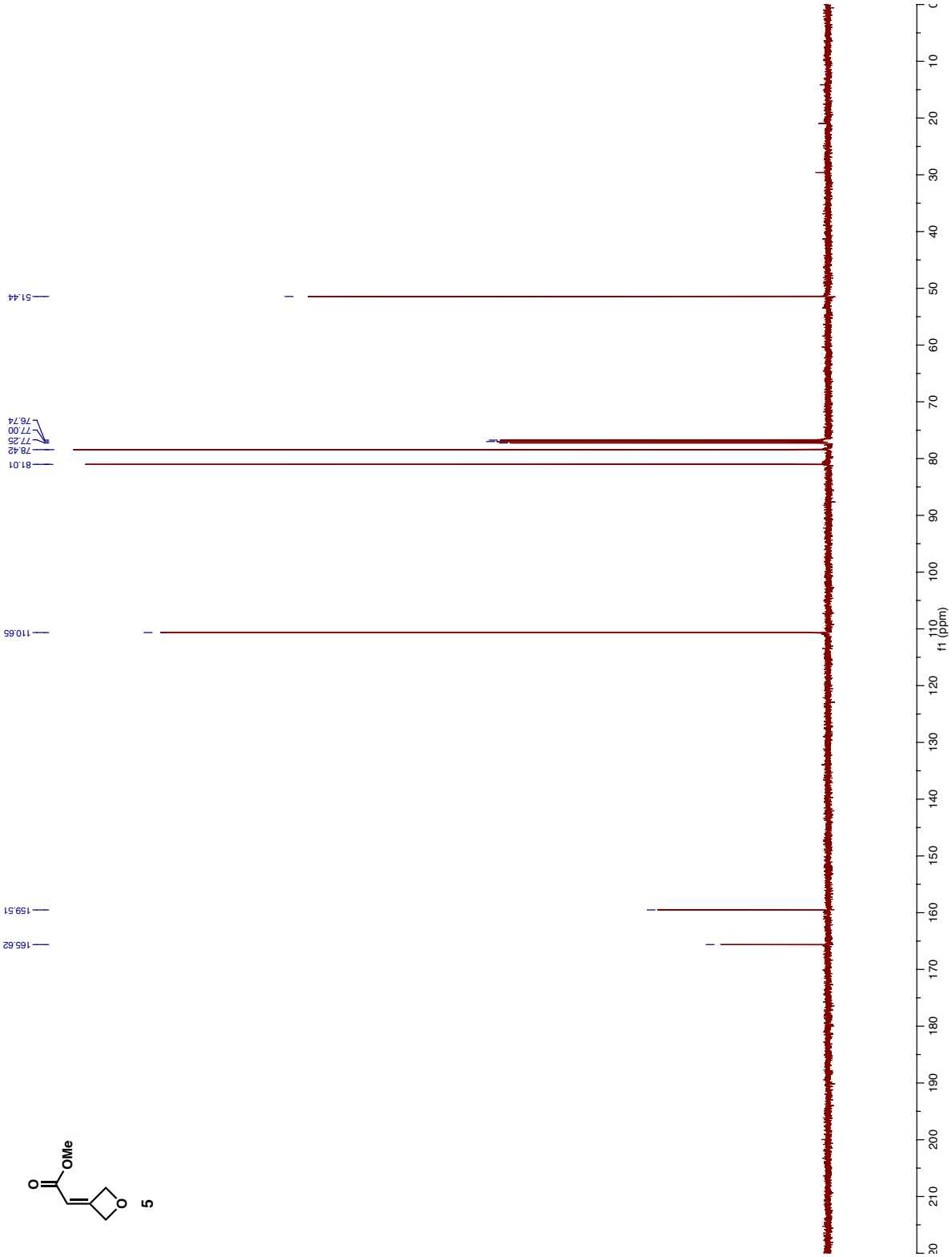
51.44
76.74
77.00
77.25
78.42
81.01
110.65
159.51
165.62
f1 (ppm)
OMe
O
O
5